Geochemistry, Geophysics, Geosystems

RESEARCH ARTICLE
10.1029/2019GC008774

Ultramafic Carbonated Melt- and Auto-Metasomatism in Mantle Eclogites: Compositional Effects and Geophysical Consequences

Sonja Aulbach[1,2], Malcolm Massuyeau[3], Joshua M. Garber[4], Axel Gerdes[1,2], Larry M. Heaman[5], and K.S. Viljoen[3]

[1]Institut für Geowissenschaften, Goethe-Universität, Frankfurt am Main, Germany, [2]Frankfurt Isotope and Element Research Center (FIERCE), Goethe-Universität Frankfurt, Frankfurt am Main, Germany, [3]Department of Geology, University of Johannesburg, Auckland Park, South Africa, [4]Department of Geosciences, Pennsylvania State University, University Park, PA, USA, [5]Department of Earth and Atmospheric Sciences, University of Alberta, Edmonton, Canada

Key Points:
- Exploration of metasomatic effects during subduction of ancient oceanic crust and after its emplacement into cratonic lithospheric mantle
- Metasomatism by kimberlite-like ultramafic melt affected between 20% and 40% of mantle eclogite suites worldwide, mostly at 2–5 GPa
- Metasomatism lowers FeO, hence density in eclogite; no significant effect on shearwave velocities

Supporting Information:
- Supporting Information S1
- Data Set S1

Correspondence to:
S. Aulbach,
s.aulbach@em.uni-frankfurt.de

Citation:
Aulbach, S., Massuyeau, M., Garber, J. M., Gerdes, A., Heaman, L. M., & Viljoen, K. S. (2020). Ultramafic carbonated melt- and auto-metasomatism in mantle eclogites: Compositional effects and geophysical consequences. *Geochemistry, Geophysics, Geosystems*, *21*, e2019GC008774. https://doi.org/10.1029/2019GC008774

Received 31 OCT 2019
Accepted 26 FEB 2020
Accepted article online 28 FEB 2020

[Correction added on 14 JAN 2021, after first online publication: Projekt Deal funding statement has been added.]

Abstract The mineralogy, chemical composition, and physical properties of cratonic mantle eclogites with oceanic crustal protoliths can be modified by secondary processes involving interaction with fluids and melts, generated in various slab lithologies upon subduction (auto-metasomatism) or mantle metasomatism after emplacement into the cratonic lithosphere. Here we combine new and published data to isolate these signatures and evaluate their effects on the chemical and physical properties of eclogite. Mantle metasomatism involving kimberlite-like, ultramafic carbonated melts (UM carbonated melts) is ubiquitous though not pervasive, and affected between ~20% and 40% of the eclogite population at the various localities investigated here, predominantly at ~60–150 km depth, overlapping cratonic midlithospheric seismic discontinuities. Its hallmarks include lower jadeite component in clinopyroxene and grossular component in garnet, an increase in bulk-rock MgO ± SiO_2, and decrease in FeO and Al_2O_3 contents, and LREE-enrichment accompanied by higher Sr, Pb, Th, U, and in part Zr and Nb, as well as lower Li, Cu ± Zn. This is mediated by addition of a high-temperature pyroxene from a UM carbonated melt, followed by redistribution of this component into garnet and clinopyroxene. As clinopyroxene-garnet trace-element distribution coefficients increase with decreasing garnet grossular component, clinopyroxene is the main carrier of the metasomatic signatures. UM carbonated melt-metasomatism at >130–150 km has destroyed the diamond inventory at some localities. These mineralogical and chemical changes contribute to low densities, with implications for eclogite gravitational stability, but negligible changes in shear-wave velocities, and, if accompanied by H_2O-enrichment, will enhance electrical conductivities compared to unenriched eclogites.

Plain Language Summary Oceanic crust formed at spreading ridges is recycled in subduction zones and undergoes metamorphism to eclogite. Some of this material is captured in the overlying lithospheric mantle, where it is exhumed by passing magmas. Having formed in spreading ridges, these eclogites have proven invaluable archives for the onset of plate tectonics, for the construction of cratons during subduction/collision, as probes of the convecting mantle from which their precursors formed, and as generators of heterogeneity upon recycling into Earth's convecting mantle. During subduction and until exhumation, interaction with fluids and melts (called metasomatism) can change the mineralogy, chemical composition, and physical properties of mantle eclogites, complicating their interpretation, but a comprehensive study of these effects is lacking so far. We investigated mantle eclogites from ancient continents (cratons) around the globe in order to define hallmarks of metasomatism by subduction-related fluids and small-volume ultramafic carbonated mantle melts. We find that the latter is pervasive and occurs predominantly at midlithospheric depths where seismic discontinuities are detected, typically causing diamond destruction and a reduction in density. This has consequences for their gravitational stability and for the interpretation of shearwave velocities in cratons.

1. Introduction

Mantle eclogites are high-pressure garnet-clinopyroxene rocks that constitute a portion of xenolith suites entrained in kimberlites worldwide, and are thought to occur as lenses, pods, or layers within cratonic

lithospheres (Helmstaedt & Schulze, 1989; Jacob, 2004). The premetamorphic origin of most of these suites as subducted oceanic crust is recognized based on elemental, isotopic, experimental, and modeling constraints (Aulbach & Jacob, 2016). Their protracted history in the cratonic mantle lithosphere—involving Precambrian oceanic crust subduction, metamorphism, and interaction with kimberlite magma prior to entrainment—suggests the possibility that their compositions have changed significantly. Such changes include interactions between slab-derived metasomatic fluids and melts with portions of the oeanic crust upon subduction ("auto-metasomatism" in the sense that the agent is internal to the slab) and/or of mantle-derived fluids and melts with the eclogite reservoir after emplacement in the mantle lithosphere ("mantle metasomatism" in the sense that the agent is externally derived). Indeed, various effects of metasomatism in eclogites have been described, such as addition of hydrous minerals or carbonates, enrichments in MgO and incompatible elements, as well as enriched isotopic compositions (e.g., Czas et al., 2018; Heaman et al., 2002, 2006; Hills & Haggerty, 1989; Huang et al., 2012, 2014; Ireland et al., 1994; De Stefano et al., 2009; Jacob et al., 2009; Misra et al., 2004; Pyle & Haggerty, 1998; Shu et al., 2018; Smart et al., 2009, 2014; Spetsius & Taylor, 2002; Taylor et al., 1996; Viljoen et al., 1996; Zedgenizov et al., 2018). Introduction or internal production of a carbonatite- or kimberlite-like ultramafic melt has been implicated in many of these instances, and such melts have been shown to be temporally and genetically related to kimberlite magmatism (e.g., Giuliani et al., 2014; Jollands et al., 2018; Yaxley et al., 2017). The ability to distinguish low-pressure (crustal) and secondary signatures is necessary for accurate interpretation within a regional tectonomagmatic framework, which has implications for eclogite origins, craton construction and evolution, and physical properties of the cratonic mantle (e.g., Shirey & Richardson, 2011).

Despite sporadic investigations of metasomatism in eclogite, a comprehensive effort to assess the compositional effects—on a minor but consequential part of the lithospheric mantle—or its pervasiveness has yet to be made. Recent research, aiming to estimate the proportion of eclogite in cratonic lithosphere, has highlighted the role of eclogite in explaining some enigmatic geophysical observations (Garber et al., 2018). However, the densities, seismic velocities, and electrical conductivities of minerals in both metasomatized and "pristine" eclogites and pyroxenites as a function of depth (and taking into account regional peculiarities) have not been systematically investigated. Here we combine published and new data for kimberlite-hosted mantle eclogite/pyroxenite suites from Orapa (Zimbabwe craton), Lace (Kaapvaal), and Diavik (Slave) with the aims to (1) identify elemental markers of UM carbonated melt metasomatism in mantle eclogite/pyroxenite that distinguish this from other types of metasomatism; (2) obtain further insights into the timing, locus, and pervasiveness of this interaction; and (3) explore physical consequences with respect to density, seismic velocity, and electrical conductivity, which may be used to refine craton-specific estimates of eclogite/pyroxenite proportions as part of the subcontinental lithosphere. These are critical to understanding and accurately interpreting the bulk lithospheric mantle signature detected geophysically, which is commonly used to infer the composition, thermal state, and structure of cratonic lithosphere, with geodynamic implications.

2. Sample Classification and Database

To understand compositional signatures of auto- and mantle metasomatism, we compiled new and published data from a global suite of cratonic mantle eclogites (Figure 1). Various criteria, based on garnet, clinopyroxene, and reconstructed bulk-rock compositions, are used to classify garnet-clinopyroxene rocks, following Aulbach and Jacob (2016) who focussed on non-metasomatized samples to capture the nature of their low-pressure protoliths. To this end, samples are divided into gabbroic (whole-rock Eu/Eu* = chondrite-normalized Eu/(Sm*Gd)^0.5 > 1.05; Rudnick & Fountain, 1995) and non-gabbroic samples to broadly separate cumulate protoliths (plagioclase-rich) from protoliths representing complementary melts, and further into pyroxenites (molar Na/(Na + Ca in clinopyroxene <0.2) and eclogites. Non-gabbroic eclogites comprise high-Ca (garnet Ca# = molar Ca/(Ca + Fe + Mg + Mn) > 0.2), high-Mg (Ca# ≤0.2 and Mg# = molar Mg/(Mg + Fe^{total}) > 0.6) and low-Mg (Ca# ≤ 0.2 and Mg# ≤0.6) varieties. Although these cut-off values do not rigorously yield separate groupings, and the classification of each individual suite must be separately evaluated, they generally reflect different protoliths and processes in unmetasomatized samples: High-Mg and high-Ca eclogites largely represent less- and more-differentiated crustal protoliths, respectively, whereas low-Mg eclogites typically require Fe-rich protoliths (Aulbach & Jacob, 2016). For the locations for which new data are presented (Diavik, Lace, Orapa), supporting information Text S1 provides an overview of prior work, samples, methods, data filtering, and a description of the results, which are

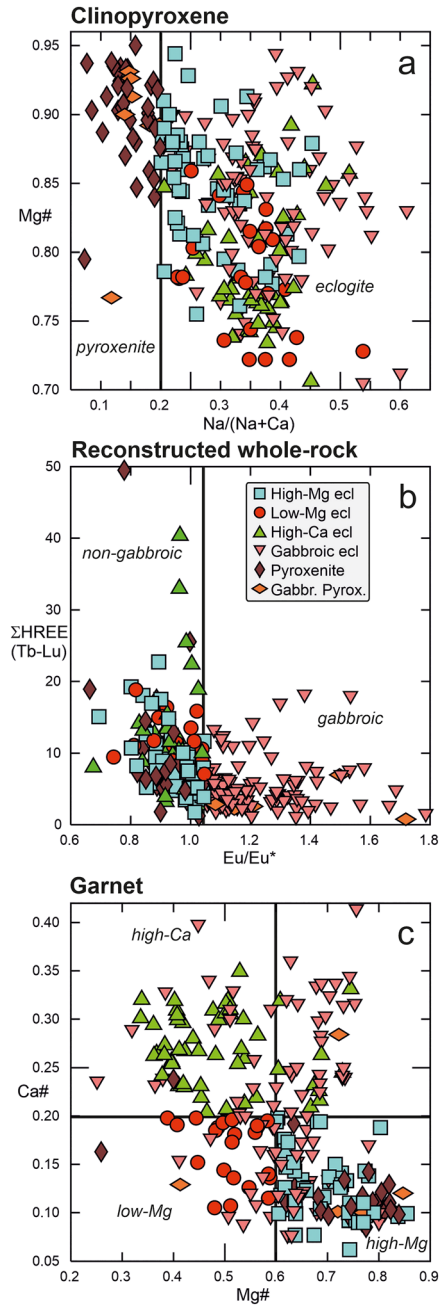

Figure 1. Criteria used to distinguish eclogite and pyroxenite classes. (a) Mg# (molar Mg/(Mg + Fe_{total}) as a function of Na/(Na + Ca) in clinopyroxene, separating pyroxenites from eclogites. (b) Total HREE content (ΣHREE, summing abundances from Tb to Lu in ppm) as a function of Eu/Eu* (chondrite-normalized Eu/(Sm*Gd)^0.5; chondrite of Sun & McDonough, 1989) in garnet, separating gabbroic from non-gabbroic eclogites and (c) Ca# (molar Ca/(Ca + Mg + Fe + Mn)) as a function of Mg#, classifying non-gabbroic eclogites into high-Mg, low-Mg, and high-Ca classes. Samples are from the northern Slave craton (Jericho, Muskox, Voyageur; Smart et al., 2009, 2014, 2017), central Slave craton (Diavik; Schmidberger et al., 2007; this study), West African craton (Koidu; Barth et al., 2001, 2002; Aulbach, Höfer, & Gerdes, 2019), Zimbabwe craton (Orapa; Viljoen et al., 1996; Aulbach et al., 2016; this study), and the Kaapvaal craton (Kimberley, Jacob et al., 2009, and Lace, Aulbach & Viljoen, 2015; Aulbach et al., 2016).

displayed in Tables S1 to S10. Literature data comprise suites from the northern Slave craton (Jericho, Muskox, Voyageur; Smart et al., 2009, 2014, 2017), Koidu in the West African craton (Aulbach, Höfer, & Gerdes, 2019; Barth et al., 2001, 2002), and phlogopite-bearing eclogites/pyroxenites from Kimberley in the Kaapvaal craton (Jacob et al., 2009), for which trace-element ± isotopic compositions are available. Comparisons are also made to eclogites from Fort a la Corne in the Sask craton (Czas et al., 2018) and to eclogites from Roberts Victor in the Kaapvaal craton (Huang et al., 2012, 2014; Radu et al., 2019). These suites have been selected because they are described as having some proportion of metasomatized samples; for the sake of clarity not all suites are shown in all figures. In the following, we will only refer to "eclogites" for brevity, with the implicit understanding that this also includes pyroxenites unless stated otherwise.

As outlined in supporting Text S1, metasomatized samples are classified based on REE patterns into LREE-enriched eclogites and HREE-enriched eclogites, the latter exemplified by phlogopite-eclogites from Kimberley, which have been enriched in both LREE and HREE, and distinguished from unenriched eclogites (Figure S1). Different types of metasomatism are recognized according to the effects they produce: Patent metasomatism entails addition of new minerals, whereas cryptic metasomatism is observable only in incompatible element composition (Dawson, 1984), and stealth metasomatism entails addition of minerals that are part of the preexisting assemblage, but with a distinct composition (O'Reilly & Griffin, 2013). Metasomatism is further distinguished according to the locus of interaction, as outlined in the introduction: auto-metasomatism, which occurs due to metamorphic reactions in subducting slabs and involves fluids and melts from various slab components, vs. mantle metasomatism (Roden & Murthy, 1985), which occurs after emplacement of eclogitized oceanic crust in the subcontinental lithospheric mantle.

3. Geothermobarometry and Bulk-Rock Reconstruction

Temperatures were derived from the garnet-clinopyroxene Mg-Fe exchange thermometer of Krogh (1988; T_{KR88}), which yields on average lower temperatures than that of Krogh Ravna (2000) (Figure S4). Barometry on mantle eclogites is hampered by the small amount of tetrahedrally coordinated Al, which is the pressure-sensitive component in clinopyroxene (Beyer et al., 2015; P_{B15}) (see Text S1). To circumvent this problem, here, pressures are estimated for all samples by iterative solution with the regional peridotite-derived conductive geotherm. For Koidu, Lace, and Roberts Victor, reported geotherms correspond to a surface heatflow of 38 mW/m^2 (Griffin et al., 2003; Mather, 2012; Smit et al., 2016). For Diavik, samples from the shallow portion of the lithosphere (to ~4 GPa) appear to have equilibrated to a lower geotherm (35 mW/m^2) than those from the deeper lithosphere (Griffin, Doyle, et al., 1999; Grütter, 2009). At the peridotite-derived geotherm for Orapa (40 mW/m^2; Stiefenhofer et al., 1997), the deepest samples were apparently derived from beyond the geophysically determined depth to the lithosphere-asthenosphere boundary (220 km; Miensopust et al., 2011), suggesting failure to equilibrate to the geotherm and isobaric heating. A gradient for a surface heat flow of 36 mW/m^2 was determined for

samples from the northern Slave craton (Grütter, 2009). With the exception of Smit et al. (2016), these works describe geothermal gradients with respect to the older family of geotherms presented by Pollack and Chapman (1977; PC77), which show too great a curvature at pressures >6 GPa in comparison to pressure-temperature arrays of cratonic mantle xenoliths (Rudnick & Nyblade, 1999). Therefore, the family of geotherms of Hasterok and Chapman (2011; HC11) is used for iterative calculations. Since even at pressures <6 GPa the two geotherm families do not coincide (Figure S4), the PC77 estimates are approximately converted to HC11, and this is done by replacing 40, 38, and 36 geotherms according to PC77 with 38, 37, and 35 geotherms according to HC11. Hasterok and Chapman (2011) determined a surface heatflow of 40.2 mW/m^2 for the Kalahari craton, without distinguishing between xenoliths entrained in Jurassic orangeites and Cretaceous kimberlites, and of 37 mW/m^2 for the Slave craton combining both northern and central Slave xenoliths. We prefer to keep these separate in accord with prior work finding distinct pressure-temperature arrays (e.g., Grütter, 2009).

Advected heat, likely connected to kimberlite magmatism, is common especially near the base of the continental lithosphere (Grütter, 2009). Such samples will have overestimated pressures if their temperatures are solved with the steady-state geotherm. This includes five samples from Orapa (OE1, 23, 26, 33, 34) and eight samples (D1056, D1530, D1503, D1541, D1534, D1617, D1649, MX121) from the deeper central Slave lithosphere, which equilibrated to a higher apparent conductive geotherm than those derived from the shallow lithosphere (Griffin, Doyle, et al., 1999; Grütter, 2009). These samples will not be considered for depth estimates (section 5.1.6) or considerations of geophysical properties (section 5.2). Iterative solutions of T_{KR88} with P_{B15}, employing only samples with clinopyroxene <1.985 Si cations per formula unit (pfu) considered to be reasonably accurate (Beyer et al., 2015), show a good positive correlation with solutions using the regional conductive geotherm, but P_{B15} may be systematically slightly underestimated, judging by the pressure-temperature arrays of individual eclogite suites relative to corresponding peridotite-derived conductive geotherms (Figure S4). For samples with clinopyroxene Si <1.985 pfu, the average difference between iterative solutions of T_{KR88} with P_{B15} and with the regional conductive geotherm is ~0.9 GPa.

Whole rock compositions were calculated for bimineralic eclogites assuming garnet and clinopyroxene modes of 55 and 45 wt%, respectively (Aulbach & Jacob, 2016). This is consistent with the average modes determined in a recent study on a large suite of eclogite xenoliths from Siberia (55.4 $\pm$ 5.1 (1σ) wt% garnet, 44.3 $\pm$ 5.0 wt% clinopyroxene; Agashev et al., 2018), and is also close to those calculated from average mantle eclogite compositions based on thermodynamic modeling at an intermediate lithospheric pressure of 4 GPa (59 and 41 wt%, respectively; Garber et al., 2018). Higher variance may be observed in other suites in particular comprising smaller sample sizes, but it is difficult to assess whether this reflects compositional variability inherited from the protoliths, or is due to a combination of typically large grain size in mantle eclogite relative to xenolith size and/or mineralogical layering. In detail, these modes will vary depending on bulk composition (e.g., basaltic vs. picritic protoliths, melt-undepleted vs. -depleted, pristine or metasomatized) and also on pressure. For example, the global-average cratonic eclogite model of Garber et al. (2018) shows ~3% modal variation between 6 and 8 GPa, whereas experimental work on subsolidus eclogites with MORB compositions and on melt-depleted eclogites shows 8% modal variations over the same pressure interval (Knapp et al., 2015). The average uncertainty in reconstructed bulk rock compositions related to 10% modal variation is given in Table 1. Additional uncertainties apply to samples containing minor mineral phases, such as kyanite or orthopyroxene. The abundance of frequently observed accessory rutile is difficult to constrain accurately or precisely in typically small (<10 cm) xenoliths, but its omission in bulk-rock reconstructions leads to an underestimate of TiO_2, Nb, and Ta concentrations (Aulbach et al., 2008). As outlined in Aulbach and Jacob (2016), the TiO_2 deficit is compensated by assuming that the bulk rock has no negative Ti anomaly relative to elements of similar compatibility during decompression melting of a dry peridotite, as applies to MORB. The amount of rutile necessary to erase such anomaly is then determined, while Zr and Hf concentrations in the hypothetical rutile are calculated using published distribution coeffients for rutile-eclogite. Concentrations will be a maximum estimate if the original rock had a negative Ti anomaly, as applies to some gabbroic eclogites with cumulate protoliths (Aulbach & Jacob, 2016), or samples that experienced LREE enrichment unaccompanied by HFSE addition. Finally, although accessory zircon and apatite occur in some eclogite suites (e.g., Heaman et al., 2006; Nikitina et al., 2014; Shchukina et al., 2018), they are relatively uncommon, and are thus not considered, as is coesite, which is generally trace element-poor and mainly dilutes the other components (Jacob et al., 2003).

Geochemistry, Geophysics, Geosystems

10.1029/2019GC008774

Table 1
Salient Compositional and Physical Characteristics of Unenriched and Metasomatized Cratonic Eclogites and Pyroxenites

Locality	Craton/kimberlite age[a]	Type	n	Reference[b]	Gradient[c]	T[c]	P[c]	d[c]	WR SiO_2	WR Al_2O_3	WR Cr_2O_3	WR FeO^{total}	WR MgO	WR CaO	WR Na_2O	WR Eu/Eu*[d]
Unit					mW/m^2	°C	GPa	km	wt%	wt%	wt%	wt%	wt%	wt%	wt%	
Eclogites and Pyroxenites																
Jericho-Muskox-Voyageur	Northern Slave/173 Ma	Unenriched	15	1–3	35	786	4.9	156	46.5	16.3	0.05	12.7	10.6	11.2	2.11	1.35
		LREE-enriched	11			742	4.3	138	47.5	13.9	0.47	5.5	18.7	11.4	0.78	0.96
Diavik	Central Slave/55 Ma	Unenriched	14	4, this work	37	915	4.4	141	47.3	15.0	0.08	8.9	13.1	12.6	1.84	1.07
		LREE-enriched	3			744	3.3	106	47.2	14.7	0.09	8.7	16.4	10.9	1.50	1.09
Koidu	West African/146 Ma	Unenriched	52	5	37	820	3.7	119	46.7	14.9	0.05	12.8	10.4	12.3	2.12	0.96
		LREE-enriched	20			770	3.5	112	47.1	14.1	0.13	9.6	15.4	11.3	1.46	0.94
Orapa	Zimbabwe/~90 Ma	Unenriched	15	this work	38	884	3.9	126	47.0	15.8	0.06	10.9	12.0	11.6	2.16	1.11
		LREE-enriched	11			721	2.9	94	46.7	15.1	0.16	10.1	14.6	11.0	1.73	1.01
Lace	Kaapvaal/132 Ma	Unenriched	46	6–7	37	906	4.3	138	47.4	16.2	0.09	8.4	13.2	10.4	2.28	0.94
		LREE-enriched	15			889	4.2	135	47.6	14.7	0.15	7.8	16.5	10.3	1.31	0.91
		Auto-metasomatized	11			919	4.4	141	47.6	16.4	0.12	7.3	14.3	10.8	2.12	0.96
Kimberley	Kaapvaal/~95 Ma	HREE-enriched	8	8	38	1041	4.9	155	45.7	14.8	0.12	11.0	11.4	13.0	1.81	0.96
		LREE-enriched	6			871	3.8	123	46.9	13.7	0.50	6.5	16.7	11.5	1.20	0.90
Kimberlite[e]									34.6	2.9	2.93	8.1	30.2	10.2	0.23	0.98
Median 10% modal uncertainty (0.55cpx + 0.45gt vs. 0.45cpx + 0.55gt)									1.5	−1.5	0.0	−1.1	−0.2	0.9	0.4	

Locality	Type	Gt grs[f]	Cpx jd[f]	Cpx Li	Cpx Ti	Cpx Sr	Cpx Y	Cpx Zr	Cpx Nb	Cpx Ce	Cpx Th	Cpx U	Cpx H_2O[g]	cpx/gt D_{Ce}[h]	rho[i]	V_s[i]
Unit				ppm	ppm	ppm	ppm	ppm	ppm	ppm	ppm	ppm	ppm		kg/m^3	km/s
Eclogites and Pyroxenites																
Jericho-Muskox-Voyageur	Unenriched	0.23	0.32	5.7	836	205	0.75	11	0.03	3.6	0.12	0.01		24	3.70	4.74
	LREE-enriched	0.11	0.10	0.3	779	469	3.78	19	1.19	56.1	0.23	0.06	333	136	3.55	4.77
Diavik	Unenriched	0.24	0.25	3.0	1589	180	1.40	6	0.01	4.4	0.01	0.00		28	3.60	4.71
	LREE-enriched	0.10	0.20	1.1	1552	436	1.94	32	0.19	38.0	0.54	0.08	398	346	3.58	4.70
Koidu	Unenriched	0.24	0.32	5.9	1040	140	1.36	21	0.02	5.7	0.04	0.02		40	3.67	4.67
	LREE-enriched	0.11	0.20	1.5	1205	251	2.51	28	0.05	24.3	0.41	0.08	415	369	3.61	4.70
Orapa	Unenriched	0.22	0.29	5.2	2386	106	1.16	13	0.12	3.6	0.01	0.00		9	3.62	4.70
	LREE-enriched	0.13	0.24	2.8	2527	324	2.14	43	0.32	39.1	0.48	0.10	505	215	3.61	4.71
Lace	Unenriched	0.17	0.32	6.7	1711	155	1.41	23	0.03	3.0	0.00	0.00		22	3.59	4.75
	LREE-enriched	0.12	0.18	5.7	1424	258	2.24	25	0.04	13.0	0.03	0.01	433	76	3.57	4.74
	Auto-metasomatized	0.14	0.30	4.8	1246	194	3.51	12	0.03	8.1	0.01	0.00	624	5	3.56	4.76
Kimberley	HREE-enriched	0.26	0.27	1.3	1875	502	4.97	92	0.95	31.6	0.29	0.02	510	32	3.65	4.65
	LREE-enriched	0.12	0.15	0.6	704	436	2.37	38	0.39	44.6	0.43	0.02	382	122	3.53	4.72

Table 1 *(continued)*

Locality	Type	Gt grs[f]	Cpx jd[f]	Cpx Li	Cpx Ti	Cpx Sr	Cpx Y	Cpx Zr	Cpx Nb	Cpx Ce	Cpx Th	Cpx U	Cpx H_2O[g]	cpx/gt D_{Ce}[h]	rho[i]	V_s[i]
Kimberlite[e]				32	6914	884	10.9	143	142	233	15	3.6	3–10 wt%			
cpx/kimberlite D_{min}[j]				0.04	0.18	0.07	0.18	0.02	0.004	0.11						
cpx/kimberlite D_{max}[j]				0.20	0.88	0.21	1.10	1.40	0.020	0.12						
Cpx in equilibrium with kimberlite$_{min}$[j]				1.4	1258	62	1.9	3	0.5	26						
Cpx in equilibrium with kimberlite$_{max}$[j]				6.4	6084	182	12.0	200	2.8	28						
Median 10% modal uncertainty on reconstructed whole-rock concentration				0.5	23	18	−2.2	0.5	0.002	0.7	0.003	0.0002				

Note. Median values are given; Cpx clinopyroxene, Gt garnet, WR whole rock reconstructed from mineral modes and compositions assuming 0.45% cpx and 0.55% gt by weight; unenriched applies to whole-rocks with NMORB-normalized Ce/Yb <1, LREE-enriched with Ce/Yb >1 and HREE-enriched with elevated contents of both LREE and HREE (see Figure S1). [a]Kimberlite ages from Davis (1977), Allsopp et al. (1989), Heaman et al. (2004, 2006), Creaser et al. (2004), Skinner et al. (2004), Becker and Le Roex (2006), Howarth et al. (2011). [b]1 = Smart et al. (2009); 2 = Smart et al. (2014); 3 = Smart et al. (2017); 4 = Schmidberger et al. (2007); 5 = Aulbach, Höfer, & Gerdes (2019); 6 = Aulbach and Viljoen (2015); 7 = Aulbach et al. (2016); 8 = Jacob et al. (2009). [c]Peridotite-derived conductive geotherm (references in main text), corresponding to a surface heatflow parameterized from Hasterok and Chapman (2011); temperature (T) and pressure (P) were derived by iterative solution of the cpx-garnet Mg-Fe exchange thermometer (Krogh, 1988) with the regional geotherm; depth (d) converted from pressure after Garber et al. (2018). Excludes five samples from Orapa and eight from the deeper Diavik lithosphere that did not equilibrate to the regional conductive geotherm (see text). [d]Eu anomaly relative to the similarly compatible elements during dry peridotite melting, gauged as chondrite-normalized Eu/(Sm*Gd)^0.5 (chondrite of Sun & McDonough, 1989). [e]Average of median compositions reported for Lace, central Slave, northern Slave and Kimberley (Hayman et al., 2009; Howarth et al., 2011; Le Roex et al., 2003; Tappe et al., 2013); range of estimated H_2O contents in parental kimberlite melts from Bell et al. (2004), Becker and Le Roex (2006), and Sokol et al. (2013). [f]Garnet grossular content (grs) and cpx jadeite content (jd). [g]Hypothetical, calculated H_2O content in cpx from LREE-enriched and HREE-enriched (Kimberley only) eclogite using the Al_2O_3-dependent cpx/melt distribution coefficient of Aubaud et al. (2008); see Figure 8 caption for details. [h]Apparent coefficient for the distribution of Ce between cpx and garnet. [i]Density (rho) and shearwave velocity (V_S) calculated from mineral endmember volumes as described in text. [j]Minimum and maximum experimental distribution coefficients reported in Klemme et al. (1995) and Blundy and Dalton (2000) and concentrations of cpx in equilibrium with kimberlite using these distribution coefficients.

4. Trace Element Homogeneity and Distribution

To assess the compositional homogeneity of the minerals, which may have been affected by entrainment in the host kimberlite and preentrainment heating and metasomatism, trace-element abundances were measured from the outermost rim to ~500 μm into the interior of touching garnet and clinopyroxene grains where possible, depending on the presence of alteration (data and supporting figures in Table S10). Two unenriched eclogites (high-Ca and low-Mg class) and two LREE-enriched eclogites (both high-Mg) from Orapa were chosen. Several spots in clinopyroxene have implausibly high Ba contents (>1 ppm) compared to Ba-poor neighboring spots and are interpreted to have been affected by kimberlite contamination in the sampled volume (Aulbach & Viljoen, 2015). The trace-element profiles show that elements that are more compatible in clinopyroxene, such as Sr and Ce, are relatively homogeneous in clinopyroxene, whereas they increase from garnet cores to rims in the two high-Mg eclogites (Table S10). Importantly, the difference in concentration between garnet and clinopyroxene in the LREE-enriched, metasomatized eclogites is systematically much larger than in the unenriched samples. This suggests that the trace-element enrichment recorded in clinopyroxene preceeded final kimberlite entrainment and related heating, which caused some diffusion of Sr, Ce, and other similarly incompatible elements into garnet, either from the clinopyroxene or from the host kimberlite or precursory melt percolation. In contrast, Y, which is more compatible in garnet than in clinopyroxene, shows no consistent zoning in either phase. As a fast-diffusing element (e.g., Dohmen et al., 2010), Li concentrations vary little in all of the grains, but are conspicuously higher in clinopyroxene from the unenriched eclogites than in those from the LREE-enriched eclogites. This broad homogeneity is suggested to reflect chemical equilibrium, and the consistent difference between LREE-enriched and unenriched eclogites is again interpreted to reflect a preentrainment event. In summary, given the small degree of variation away from the outermost rim (see typically small relative standard deviations for trace element abundances obtained from multiple spots and grains per sample in Table S5), the samples are considered to be in trace-element equilibrium, allowing distribution coefficients ($^{clinopyroxene/garnet}D_{element}$) to be calculated and interpreted with respect to their dependence on temperature (and pressure along the conductive geotherm) and composition.

5. Discussion

5.1. Compositional and Mineralogical Effects

5.1.1. Effects of Mantle and Auto-Metasomatism on Trace-Element Distribution

The compositional dependence of clinopyroxene-garnet trace-element distribution in eclogite has been previously highlighted (Aulbach et al., 2016; Harte & Kirkley, 1997; O'Reilly & Griffin, 1995). In the eclogite suites under consideration here, the jadeite and grossular components are lowest (jadeite < 0.2;

Ca# < 0.15) in LREE-enriched samples (Figure 2a). Focusing on the dependence of trace-element distribution on the grossular component to illustrate the effect of LREE-enrichment, it is evident that with decreasing garnet Ca contents, elements that are compatible (Y), mildly incompatible (Sr), and strongly incompatible (Ce) in garnet are increasingly partitioned into clinopyroxene (Figures 2b–2d). The distribution takes on a natural logarithmic form (Harte & Kirkley, 1997), such that very high values are attained for low garnet Ca#. Since UM carbonated melt metasomatism decreases garnet Ca# and the partitioning of incompatible trace elements into garnet is limited at low Ca#, this leads to the apparently paradoxical observation that garnet in LREE-enriched samples shows few—if any—trace-element differences compared to unenriched samples (Figures 2e and 2f). This is also evident from Figure S2 where REE patterns of garnet in LREE-enriched and unenriched samples from Orapa are similar but those of clinopyroxene are distinct. This illustrates that clinopyroxene is the main carrier of the metasomatic signature in LREE-enriched eclogites.

5.1.2. Patent and Stealth Effects of Mantle and Auto-Metasomatism

As outlined above, metasomatism can lead to patent, cryptic, and/or stealth effects (O'Reilly & Griffin, 2013). The most commonly described examples of patent mantle metasomatism in mantle eclogite or pyroxenite are the addition of amphibole, phlogopite, apatite, zircon, and/or carbonate and diamond as well as the appearance of melt pools, unequilibrated microstructures, and an increase in fluid inclusions (Heaman et al., 2002, 2006; Hills & Haggerty, 1989; Huang et al., 2012, 2014; Jacob et al., 2009; Misra et al., 2004; Pyle & Haggerty, 1998; Smart et al., 2009; Spetsius & Taylor, 2002). Rutile and sulphide may be metasomatic (e.g., Hills & Haggerty, 1989), but can be primary minerals, as rutile saturates during metamorphism of oceanic crust (e.g., Gaetani et al., 2008), and sulphide may be inherited from the sulphide-saturated oceanic crust (e.g., Patten et al., 2013). In contrast, zircon formation in mantle eclogite xenoliths from the Grib kimberlite in the East European platform was an auto-metasomatic process, linked to fluids emanating from a Palaeoproterozoic subduction zone (Shchukina et al., 2018). This may also apply to zircon and Nb-rich rutile in a group of mantle eclogites from Jericho recording crystallization ages close to the time of ca. 1.8 Ga metamorphism (Heaman et al., 2006). Stealth metasomatism has been recognized (though not referred to as such) in eclogites from Diavik and Ekati in the central Slave craton, expressed as the addition or overgrowth of garnet from deserpentinization fluids (Aulbach et al., 2011). At Lace in the Kaapvaal craton it is expressed as the addition of aluminous clinopyroxene precipitated from a sediment-derived melt in a subduction mélange. This clinopyroxene later exsolved garnet and kyanite (Aulbach et al., 2016). At Koidu in the West African craton, it is expressed as addition of diopside-rich clinopyroxene from a UM carbonated melt, which converted low-Mg and gabbroic eclogites to high-Mg eclogites and pyroxenites (Aulbach, Höfer, & Gerdes, 2019).

A metasomatic agent containing a sufficient amount of solutes to effect patent or stealth mineral growth should also cause significant changes in whole-rock major-element and mineralogical compositions. The major-element relationships of the various eclogite suites examined here indicate that many of the LREE-enriched samples are MgO- and Cr_2O_3-rich (Figure 3a), with high CaO compared to near-primary MgO-rich mantle melt products (Figure 3b). Those with the highest MgO contents also tend to show the highest SiO_2 contents (Figure 3c) and low FeO, Al_2O_3, and Na_2O (Figures 3d–3f). These changes are explainable by addition of a high-temperature pyroxene from an external UM carbonated melt, such as those reported in Mallik and Dasgupta (2013) and shown in Figure 15 in Aulbach, Höfer, and Gerdes (2019). In particular, we interpret the anticorrelation of MgO with FeO (Figure 3d) and correlation with SiO_2 at high MgO contents as a pyroxene control line (Figure 3c). If so, the modes assumed for LREE-enriched samples may be better represented by higher clinopyroxene modes of, e.g., 50% than the 45% used to reconstruct bulk rocks. This is because not all added components can be equally accommodated by garnet (in particular, SiO_2 or Na_2O) and need to be added as more cpx. We account for this by considering, hypothetically, the effect of addition of 5% eclogitic clinopyroxene. The uncertainty resulting from a 10% modal variation (i.e., 45% clinopyroxene-55% garnet and 55% clinopyroxene-45% garnet) is displayed in Figure 3 and, with the exception of SiO_2, is small relative to the variation displayed. An increase in clinopyroxene mode by 5% would shift the bulk rock up by half the length of the error bar with respect to SiO_2, Na_2O, and CaO and down with respect to FeO and Al_2O_3 at nearly constant MgO and Cr_2O_3. More drastic changes in garnet-clinopyroxene modes appear unlikely because high-MgO eclogites and low-MgO eclogites have indistinguishable modal proportions, e.g., in the Koidu suite (Hills & Haggerty, 1989). Even if a high-temperature pyroxene was added, reequilibration with the preexisting assemblage is indicated by concomitant changes in

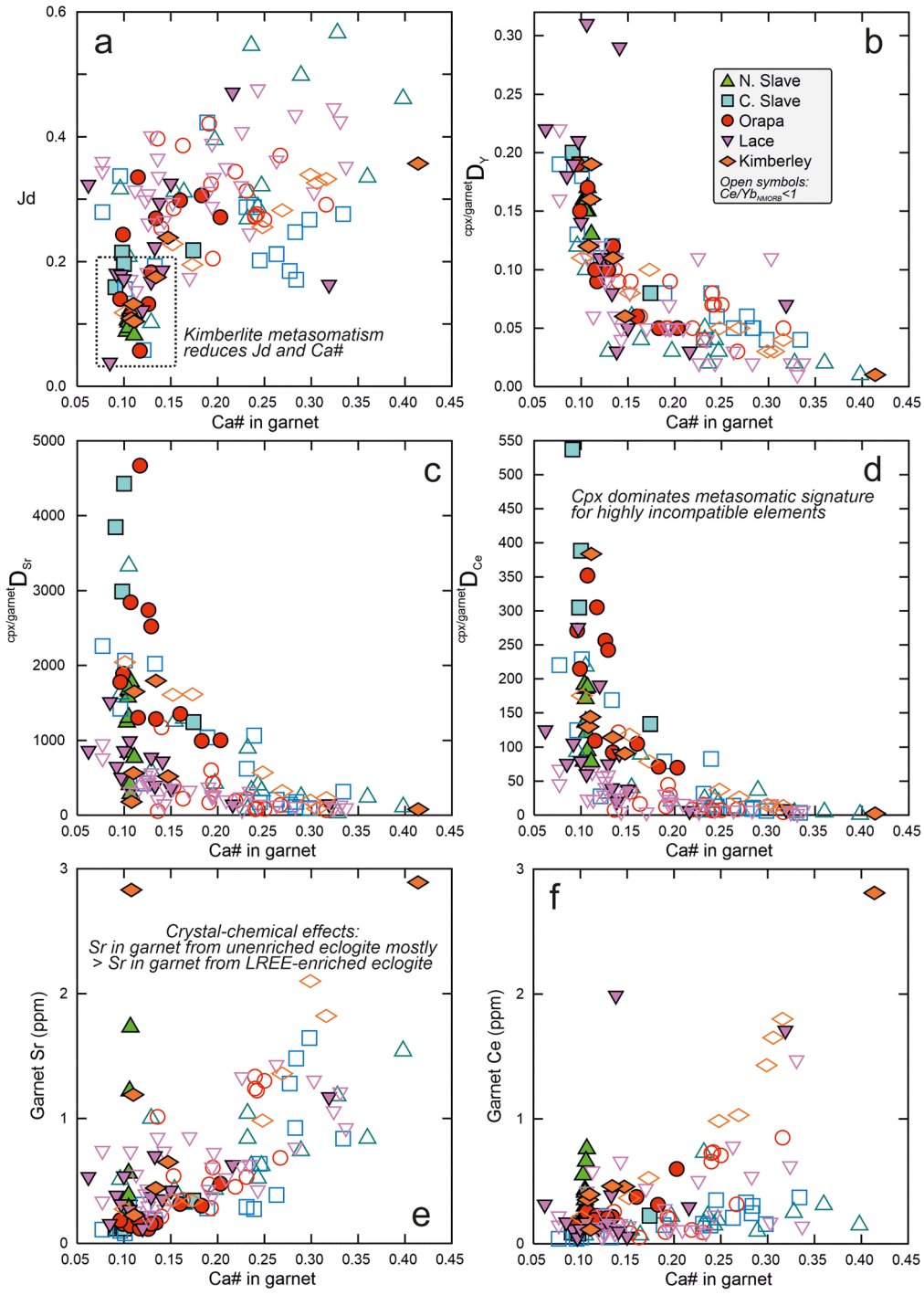

Figure 2. Effects of mantle metasomatism with LREE-enrichment, ascribed to interaction with a UM carbonated melt similar to kimberlite, on mineral compositions and trace-element distribution in mantle eclogites. (a) Jadeite-content in clinopyroxene as a function of grossular content (Ca#: 100Ca/(Ca + Fe + Mg + Mn) in garnet. Note the generally low values observed for LREE-enriched bulk rocks (filled symbols). (b–d) Distribution of various trace elements between clinopyroxene and garnet, expressed as $D_i = {}^{clinopyroxene}C_i/{}^{garnet}C_i$, as a function of grossular content in garnet. With decreasing garnet Ca#, all trace elements partition more strongly into clinopyroxene than into garnet; D_i become extreme for highly incompatible elements (Ce) in LREE-enriched samples with grossular-poor garnet. (e–f) Sr and Ce concentration in garnet as a function of garnet Ca#, illustrating that absolute concentrations of incompatible elements are as high or higher in unenriched eclogites and pyroxenites than in LREE-enriched eclogites, due to decreased partitioning into garnet at metasomatically induced low Ca#. Filled symbols are for LREE-enriched samples (NMORB-normalized Ce/Yb >1; NMORB from Gale et al., 2013) and open symbols for unenriched samples, except Kimberley where open symbols show samples enriched in both LREE and HREE. References as in Figure 1.

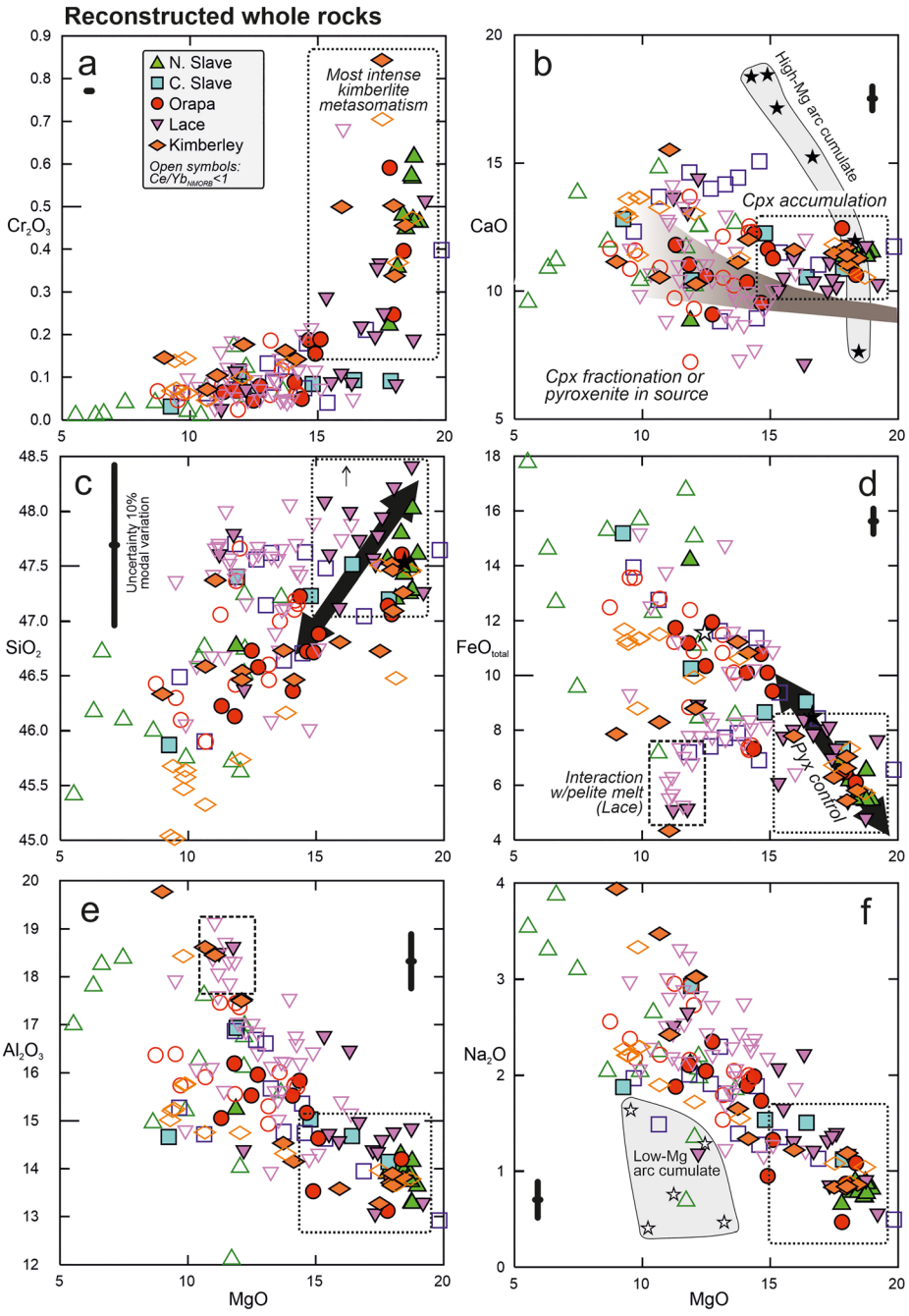

Figure 3. Effects of mantle metasomatism with LREE-enrichment, ascribed to interaction with a UM carbonated melt similar to kimberlite, on major-element systematics of mantle eclogites. Concentrations of various oxides (wt%) as a function of MgO in reconstructed eclogites and pyroxenites from various localities. In (a), stippled rectangle highlights LREE-enriched samples at generally high MgO contents. Error bar next to panel letters is for a total of 10% modal variation (e.g., 45% clinopyroxene + 55% garnet to 55% clinopyroxene + 45% garnet). Dark gray field in (b) shows expected range of MgO-CaO for primitive mantle-derived melts that experienced various degrees of fractional crystallization (Herzberg & Asimow, 2008). Fields for high-Mg and low-Mg arc cumulates (Lee et al., 2006) in panels (b) and (f), respectively, illustrate that mantle eclogites are unlikely to represent delaminated lower crustal arc material. Square with long stipples in (d) and (e) highlights samples from Lace inferred to have reacted with a sediment-derived melt in a subduction mélange, which lowered their FeO and MgO and increased their Al_2O_3 content. The correlation with SiO_2 and anticorrelation with FeO at high MgO in (c) and (d), respectively, is interpreted as a pyroxene-control line, reflecting the addition of FeO-poor and MgO-rich magmatic pyroxene further characterized by low Na_2O, moderately higher CaO and SiO_2, and higher Cr_2O_3 than the premetasomatic bulk rock. Filled symbols are for LREE-enriched samples (NMORB-normalized Ce/Yb >1; NMORB from Gale et al., 2013) and open symbols for unenriched samples, except Kimberley where open symbols show samples enriched in both LREE and HREE. References as in Figure 1.

both garnet and clinopyroxene, as, e.g., both have higher MgO and lower FeO contents. Auto-metasomatized eclogites from Lace show CaO-Al_2O_3 enrichment and FeO-MgO dilution (Figures 3d and 3e).

5.1.3. Mantle and Auto-Metasomatism and Diamond

Diamond in eclogite is regarded as a metasomatic mineral because the direct conversion of intrinsic carbon in oceanic crust is kinetically inhibited, and influx of fluids or melts is required for diamond growth (Stachel & Luth, 2015). As diamond formation involves the migration of melts and fluids containing various carbon species and abundances as a function of pressure, temperature, and oxygen fugacity (Stachel & Luth, 2015), there are varied relationships between metasomatism and the formation and stability of diamond. The close temporal relationship between eclogitic diamond formation or growth and accretionary or collisional processes during craton amalgamation or at craton margins (Shirey & Richardson, 2011; Timmerman et al., 2017) suggests an auto-metasomatic origin of diamond accompanying recycling of oceanic crust, as recognized in the central Slave craton and at Lace (Aulbach et al., 2011, 2016). This constitutes an efficient process to achieve high diamond modes, aided by the high volume of carbonaceous fluids and melts present in this tectonic setting (e.g., Poli, 2015; Tumiati et al., 2017). Moreover, the low oxygen fugacity of eclogitized oceanic crust (Smart et al., 2017; Aulbach, Woodland, et al., 2017; Aulbach, Woodland, et al., 2019) may cause CO_2 in the auto-metasomatic fluid to be reduced to diamond.

An auto-metasomatic origin for some eclogitic diamond suites does not preclude that significant new diamond growth or overgrowth on preexisting diamond can occur during later metasomatic events (e.g., Taylor et al., 1996, 1998). Although eclogitic diamond can form from reduced or mixed carbon species (Smit et al., 2019), oxidized carbon is inferred to be involved in diamond formation during interaction with oxidizing UM carbonated melts, such as kimberlite (Fedortchouk & Canil, 2004). It has also been shown that melts with dilute CO_2 content, such as kimberlite, can coexist with diamond to low fO_2 where fluids would be water-maximum (Luth & Stachel, 2014; Stagno et al., 2013; Stamm & Schmidt, 2017). Thus, diamond in eclogite from Siberia has been linked to mantle metasomatism involving UM carbonated melts or high-density fluids. This model is supported by the occurrence of diamonds in secondary alteration zones in eclogite (Schulze et al., 1996; Shatsky et al., 2008; Taylor et al., 2000; Zedgenizov et al., 2018). Carbonatitic to silicic fluids have been identified in cloudy or fibrous diamond with eclogite inclusions (Izraeli et al., 2001; Weiss et al., 2009, 2015). In the Slave craton, interaction with a UM carbonated melt produced extremely diamond-rich high-Mg eclogites or pyroxenites (Smart et al., 2009), and it has been suggested based on experimental observations that both monocrystalline and fibrous lithospheric diamonds form by redox reactions from carbonated fluids or melts (Bureau et al., 2018). Conversely, in mantle eclogites from Orapa and Koidu, the diamond-destructive nature of UM carbonated melt metasomatism is indicated by the association of diamond with high-Ca and low-Mg eclogites, but absence in LREE-enriched high-Mg eclogites and pyroxenites (Aulbach, Jacob, et al., 2017; Aulbach, Woodland, et al., 2019). Indeed, it has been shown experimentally that interaction with oxidizing small-volume carbonated silicate melts, such as kimberlite, eventually causes diamond resorption and associated carbon remobilization at mantle depth (Fedortchouk et al., 2019). These seemingly contrasting observations may relate to the local buffering capacity and fO_2 in the system. Given the aforementioned low fO_2 of mantle eclogites, the mechanism causing the observed diamond resorption by kimberlite-like melts remains unclear.

The association of diamond with high Na_2O in eclogitic garnet, whereas eclogites with low-Na_2O garnet are barren (McCandless & Gurney, 1989), has been explained by the pressure-dependent incorporation of Na_2O in garnet, as exemplified by the eclogite suite from Kaalvallei, Kaapvaal craton (Viljoen et al., 2005). Since UM carbonated melt metasomatism lowers the jadeite component in clinopyroxene and therefore bulk-rock Na_2O (Table 1), the diamond-destructive effect of metasomatism, especially near the top of the diamondiferous lithosphere, may also play a role. On the simplistic assumption that all LREE-enriched eclogites at Orapa and Koidu are barren, whereas all unenriched eclogites are diamondiferous, ~20% to 40% of the eclogitic diamond inventory was destroyed due to UM carbonated melt metasomatism. This also has physical ramifications as the absence or presence of just a few vol% diamond can significantly affect the bulk shear velocity of eclogite (Garber et al., 2018), as will be explored further below.

5.1.4. Cryptic Effects of Mantle and Auto-Metasomatism

Two types of auto-metasomatism in subduction settings have been described. Stepped REE patterns in mantle eclogites from the central Slave craton are very similar to those reported for some Phanerozoic orogenic eclogites and are inconsistent with melt depletion; they may result from garnet overgrowths due to

interaction with deserpentinization fluids, where LREE are strongly excluded and removed with the fluids (Aulbach et al., 2011). At Lace, kyanite- and/or diamond-bearing eclogites—formed through interaction of a pelite-derived melt with subducted oceanic crust in a mélange setting—show enrichments in LREE and Th, and depletions in Y, Zr, Hf, and HREE (Aulbach et al., 2016). Strong Pb addition during this event, resulting in low U/Pb for some eclogites, has allowed the retention of highly unradiogenic clinopyroxene Pb isotopic compositions ($^{206}Pb/^{204}Pb < 14$), yielding ca. 3.0 Ga single-stage model Pb-Pb ages (Aulbach, Heaman, et al., 2019). Because of the close temporal relationship of zircon crystallization in eclogite xenoliths from the northern Slave craton and Eastern European Platform with accretionary processes (Heaman et al., 2006; Shchukina et al., 2018), the HFSE enrichment accompanying zircon formation is also suggested to reflect an auto-metasomatic process unrelated to mantle metasomatism sensu stricto.

Cryptic metasomatism involving UM carbonated melts has been widely recognized, based, inter alia, on LREE ± LILE- and HFSE-enrichment (e.g., Czas et al., 2018; Heaman et al., 2006; Huang et al., 2012; Jacob et al., 2009; Smart et al., 2009). Volumes sampled during laser ablation can comprise extraneous kimberlite material in optically invisible cracks or otherwise altered material; however, as outlined in Text S1, rigorous reduction of the data with respect to such kimberlite contamination ensures that the enrichments discussed here have a preentrainment origin. The coupled enrichment of LREE and MgO in the reconstructed whole rocks (Figure 4a) clearly supports the addition of both from a small-volume (hence strongly incompatible element- and volatile-enriched) UM carbonated melt, probably from the kimberlite-carbonatite spectrum, which will be referred to here as "kimberlite-like" for simplicity. Focusing on clinopyroxene as the main carrier of the metasomatic signature, as discussed above, Pb, Th, and U were enriched along with LREE in all suites (Figures 4b and 4c), with Lace showing the lowest degree of incompatible element enrichment. Again, with the exception of Lace, Nb concentrations are on average higher in LREE-enriched eclogites (Figure 4d), whereas Zr is only enriched in some samples from Diavik and most samples from Orapa (not shown). Similarly, TiO_2 and Y are not consistently co-enriched with LREE, but concentrations of both are elevated in HREE-enriched eclogites from Kimberley, whereas clinopyroxene in LREE-enriched Orapa eclogites has higher Y but not TiO_2 contents (Figure 4e). The absence of TiO_2 and Y enrichments results from their low concentrations in kimberlite-like melts, even if elevated experimental mineral-melt partition coefficients for clinopyroxene are assumed (Table 1). In detail, such coefficients can vary significantly, and enrichment or dilution depends on trace element contents, e.g., inherited during the low-pressure history of the sample (prior to metasomatism) and degree of enrichment of the kimberlite-like melt, which may grade into basanite or carbonatite. In addition, selective TiO_2 enrichment, e.g., via ilmenite addition, would not necessarily be detected in small samples and would not show up in bulk rocks reconstructed with only garnet and clinopyroxene. Compared to only LREE-LILE enrichment ascribed to small-volume UM carbonated melt metasomatism, coupled TiO_2-Y-Zr-LREE-HREE enrichment is suggested to indicate the involvement of a higher melt fraction with more dissolved SiO_2—a silicate melt analogous to that causing "melt metasomatism" recognized in peridotites (Griffin, Shee, et al., 1999). Although the enrichment patterns vary in detail, it appears that metasomatic intensity increases from Lace to Diavik, Jericho, and Orapa, with the strongest enrichment in high-temperature HREE-enriched phlogopite-bearing eclogites from Kimberley. This is also mirrored in REE patterns of clinopyroxene in LREE-enriched eclogites, which converge with those in unenriched eclogites at Nd or Sm for Diavik, but at Ho or Er for Orapa (Figure S2). Since kimberlites have considerably higher contents of Sr, Nb, LREE, Ta, Pb, Th, and U, and to a lesser degree Zr and Hf than unenriched eclogites (Table 1), they are considered likely agents for the cryptic enrichment observed in LREE-enriched eclogites.

A puzzling characteristic of LREE-enriched eclogites is their low Li, Cu, and in part Zn abundances, as reflected in clinopyroxene (Figure 4f; Table 1) and reconstructed whole rocks, lower than expected in fresh or seawater-altered MORB (Jenner & O'Neill, 2012; Staudigel, 2005). These elements are mildly incompatible during differentiation of the inferred oceanic crustal protoliths and would therefore be expected to have low abundances in less-differentiated high-MgO and gabbroic (cumulate) protoliths, in particular at higher melt fractions facilitated by higher Archaean T_P. Nevertheless, the association of low Li, Cu, and Zn not only with high MgO but also with LREE-enrichment suggests a link to metasomatism. This implies that they were either leached out of eclogites due to low mineral-melt distribution coefficients, or diluted by stealth magmatism via addition of Li-, Cu-, and Zn-poor clinopyroxene. Lithium concentrations in kimberlite/orangeite are seldom reported; taking that from Lace with ~30 ppm (Howarth et al., 2011) as

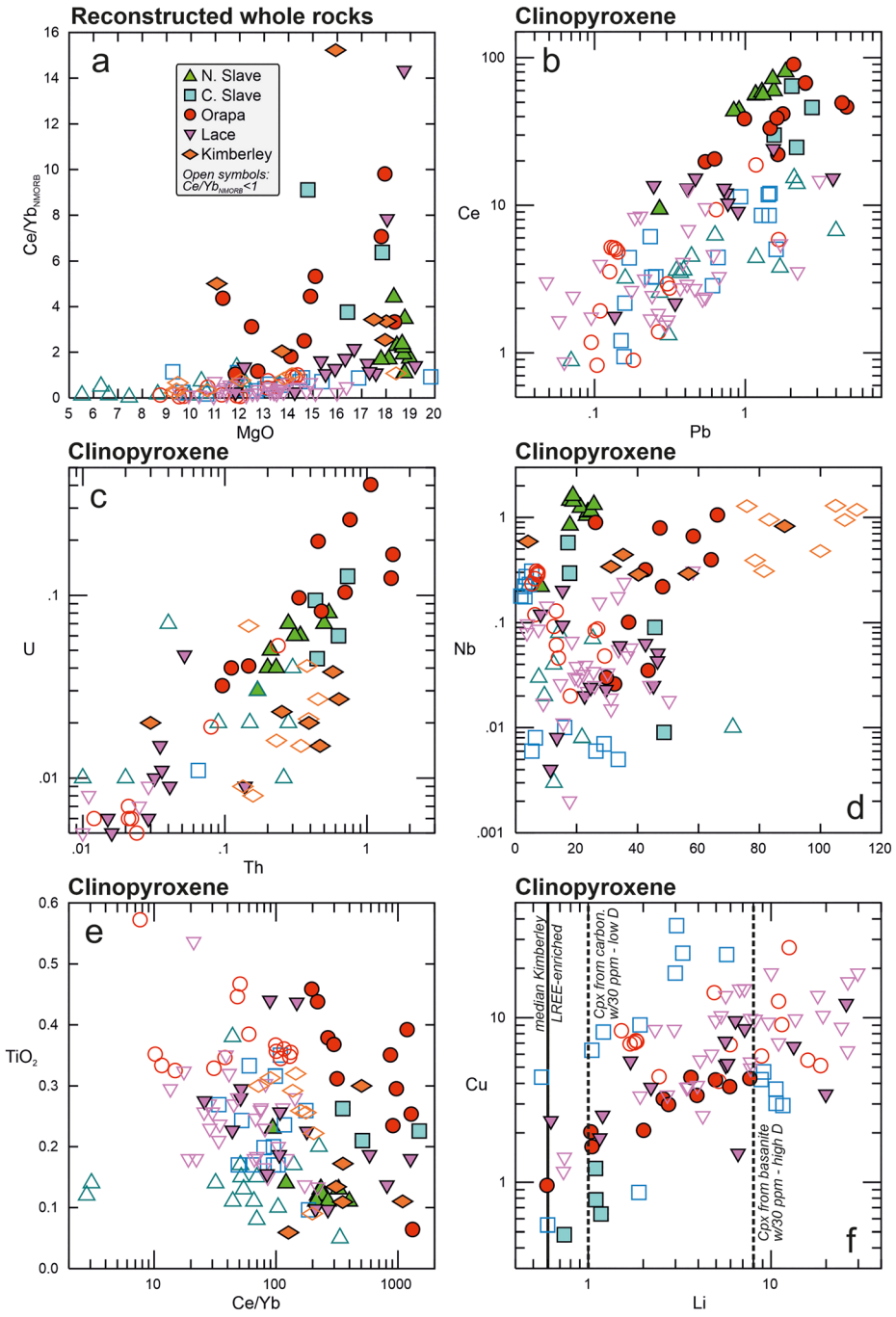

Figure 4. Cryptic effects of mantle metasomatism with LREE-enrichment, ascribed to interaction with a UM carbonated melt similar to kimberlite, on mantle eclogites. (a) NMORB-normalized Ce/Yb as a function of MgO (wt%) in reconstructed whole rocks, illustrating that LREE-enrichment is linked to an increase in MgO. (b–f) Minor- (wt%) and trace-element (ppm) relationships in clinopyroxene, as the main carrier of the metasomatic signature (see Figure 2). LREE-enrichment is accompanied by enrichment in Sr, Nb, Ce, Pb, Th, and U in most eclogite suites, whereas Y and Zr are only enriched in some. Enrichment in Y, HREE, and HFSE is ascribed to interaction with a low-volume mafic silicate melt. In contrast, TiO_2 is not higher in LREE-enriched than in unenriched samples. Copper and Li were diluted by addition of low-Li pyroxene or were leached out of the rock, in particular Kimberley (Cu is not reported) for which median Li is shown as solid line. Stippled lines show expected Li concentrations in clinopyroxene in equilibrium with melt using high ($D = 0.27$, in equilibrium with basanite; Adam & Green, 2006) and low ($D = 0.04$, in equilibrium with carbonatite "carbon."; Blundy & Dalton, 2000) experimental distribution coefficients ("D"). Filled symbols are for LREE-enriched samples (NMORB-normalized Ce/Yb >1; NMORB from Gale et al., 2013) and open symbols for unenriched samples, except Kimberley where open symbols show samples enriched in both LREE and HREE. References as in Figure 1.

representative, ~1 to 8 ppm would be expected in clinopyroxene for D = 0.04 and 0.27, respectively, as reported for equilibrium with carbonatite (Blundy & Dalton, 2000) or basanite melts (Adam & Green, 2006) (Figure 4h). Zinc and Cu may be mildly incompatible or compatible ($^{clinopyroxene/basanite}D_{Zn}$ of 0.25 to 0.69 and D_{Cu} 0.47 to 1.5, respectively; Adam & Green, 2006). Median Zn and Cu concentrations in kimberlites/orangeites from Lace, Jericho, Lac de Gras, and southern Africa vary from 38 to 75 and 50 to 77 ppm, respectively (Howarth et al., 2011; Le Roex et al., 2003; Tappe et al., 2013), compared to ~40 to 100 and 2.2 to 8.5 ppm (median) in unenriched eclogite from various suites (Table 1). Thus, precipitation of stealth clinopyroxene (and garnet) or equilibration of eclogitic minerals with kimberlite may explain the low observed Li, and perhaps Zn, concentrations in clinopyroxene from eclogites inferred to have interacted with a small-volume UM carbonated melt. The low Cu concentrations may imply sulphide precipitation from melt or fluid in the system, consistent with the near-ubiquity of this mineral in eclogite xenoliths (personal observation) and evidence for partial metasomatic origin (Aulbach et al., 2009, Aulbach, Höfer, & Gerdes, 2019).

Type I eclogites from Roberts Victor have microstructures interpreted as reflecting disequilibrium (rounded garnet grains in a "matrix" of clinopyroxene) whereas Type II eclogites have equilibrium microstructures with interlocking garnet and clinopyroxene grains, lower Na_2O in garnet and K_2O in clinopyroxene (MacGregor & Carter, 1970; McCandless & Gurney, 1989). Type I eclogites have been suggested to be the product of carbonated melt metasomatism of Group II eclogites (Huang et al., 2012, 2014), but they do not bear the hallmarks of such metasomatism identified above: Few are LREE-enriched relative to the HREE, their HREE contents are lower than those of HREE-enriched eclogites from Kimberley and eclogitic clinopyroxenes are not consistently jadeite-poor nor do they have high Mg#. Both groups display strong relationships between Eu/Eu* and total HREE contents indicative of low-pressure accumulation and fractional crystallization as exemplified by MORB (e.g., Gale et al., 2013; Jenner & O'Neill, 2012) and gabbros (e.g., Hart et al., 1999), albeit at a different slope perhaps reflecting lower oxygen fugacities (Aulbach & Viljoen, 2015) (Figure S3). Recent analysis of a large suite of Group II eclogites (Radu et al., 2019) shows that their whole-rock REE patterns, clinopyroxene K_2O contents, and garnet Na_2O contents overlap those of Group I eclogites investigated by Huang et al. (2012, 2014). We suggest that the compositional signatures (LREE-depletion, HREE-enrichment, low Sr, Na_2O, and K_2O) of Type II eclogites are mostly explained by partial melt loss and that many Type I eclogites are, in fact, relatively pristine, although we concur with Radu et al. (2019) that the relationship between the different eclogite types at Roberts Victor is not straightforward.

5.1.5. Muting of Crustal Signatures and Isotopic Effects of UM Carbonated Melt Metasomatism

LREE-enriched eclogites are dominated by high-Mg eclogites and pyroxenites, and the difference between metasomatized and unmetasomatized pyroxenite varieties tends to be small (Table 1). This suggests that part of the high-Mg eclogites and most pyroxenites are the product of metasomatism. This may be accompanied by a muting or complete erasure of typical crustal signatures. The effects of mantle metasomatism on stable or radiogenic isotope compositions have been previously discussed in the literature, with varying conclusions, and are reviewed here together with the effects on Eu/Eu* as a typical crustal signature in particular in eclogites with gabbroic protoliths. If the inference of stealth metasomatism by addition of clinopyroxene from an ultramafic kimberlite-like melt is correct, the added clinopyroxene had no or small negative Eu anomalies. Taking Ce/Yb as a measure for the intensity of UM carbonated melt metasomatism and clinopyroxene as the main carrier of the metasomatic signature, it is evident that the range of Eu/Eu* is much larger at low Ce/Yb than at high Ce/Yb (Figure 5a). When plotted against MgO content in reconstructed bulk rocks, NMORB-normalized Eu/Eu > 1.05 is retained in some gabbroic eclogites with moderate MgO contents, but in most samples with MgO >15 wt%, reflecting the greatest stealth and cryptic metasomatic overprint, Eu/Eu* is <1.05 (Figure 5b). These systematics indicate erasure of the gabbroic signature in eclogites strongly affected by mantle metasomatism, possibly aided by the experimentally demonstrated higher Eu diffusivity relative to other REE under reducing conditions (Szumila et al., 2019), such as those recorded by mantle eclogite (Aulbach, Woodland, et al., 2017, Aulbach, Woodland, et al., 2019; Smart et al., 2017; Stagno et al., 2015).

Oxygen isotope compositions lower and higher than the canonical mantle range (5.1–5.9; Mattey et al., 1994) have been interpreted as reflecting high- and low-temperature seawater alteration, respectively (Muehlenbachs & Clayton, 1972a, 1972b), although mantle-like $\delta^{18}O$ is not evidence against a

low-pressure origin (e.g., Gregory & Taylor, 1981; Smart et al., 2012). Though Huang et al. (2014) see evidence for an increase in $\delta^{18}O$ in response to mantle metasomatism in Type I eclogites at Roberts Victor, Riches et al. (2016) concluded that there is no detectible effect of metasomatism on $\delta^{18}O$ and Korolev et al. (2018) consider the effect to be small (generally <1.2‰). As discussed by Radu et al. (2019), mass balance requires high fluid/melt-rock ratios to change the isotopic composition of the major element O. Since $\delta^{18}O$ in garnet from unenriched eclogites from the northern Slave, Lace, and Koidu kimberlites are largely within the canonical mantle range, they cannot be used to assess the effect of mantle metasomatism. There is, however, some evidence that this has occurred in the sample suite from Orapa, where mantle-like $\delta^{18}O$ is associated with radiogenic Sr ascribed to overprint by a small-volume melt derived from an aged lithospheric mantle metasome (Aulbach et al., 2017). Figure 3a shows that UM carbonated melt metasomatism is accompanied by an increase in Cr_2O_3, suggested to reflect stealth addition of Cr_2O_3-rich pyroxene. This component has been taken up by both eclogitic clinopyroxene and garnet. Thus, taking Cr_2O_3 in garnet as a proxy for the degree of metasomatic alteration, it is evident that many unenriched eclogites have mantle-like $\delta^{18}O$ and some LREE-enriched mantle eclogites retain $\delta^{18}O$ outside canonical mantle, but that at high metasomatic intensity (high Cr_2O_3) values are exclusively mantle-like (Figure 5c). The association of low $\delta^{18}O$ and high Eu/Eu* in some metasomatized eclogites from the Sask craton (reported in Czas et al., 2018) appears consistent with a deep crustal gabbroic protolith that experienced high-temperature seawater alteration (not shown), whereas metasomatized samples with high MgO content have heavier, mantle-like $\delta^{18}O$, consistent with muting of the crustal signature during strong metasomatism by a UM carbonated melt (Figure 5d). Czas et al. (2018) identify chemical gradients, including in $\delta^{18}O$, from primary to metasomatized zones in eclogitic garnet in this sample suite, showing conclusively that O isotopes can be modified at high melt/rock ratios, but only toward and not away from canonical mantle values.

Effects of mantle metasomatism on radiogenic isotopes have been recognized and must be considered on a suite-by-suite basis because of local variations in the isotopic composition of the metasomatic agent, the timing of metasomatism with consequent isotopic ingrowth, and the low-pressure history of the samples. Thus, positive trends of Y and negative trends of Eu/Eu* with $^{87}Sr/^{86}Sr$ may result from accumulation (low time-integrated Rb/Sr, low Y, high Eu/Eu*) and differentiation (high time-integrated Rb/Sr, high Y, low Eu/Eu*), as discussed for Orapa (Aulbach, Jacob, et al., 2017) (Figure 6a). Interaction with a young kimberlite-like (sensu stricto) agent with OIB-like isotopic characteristics (Becker & Le Roex, 2006; Tappe et al., 2017) would increase low $^{87}Sr/^{86}Sr$ of eclogites with ancient cumulate protoliths, but decrease that of those with ancient evolved protoliths. Proto-kimberlite and orangeite metasomatism mobilizes aged and isotopically evolved lithospheric metasomes with enriched isotope characteristics (unradiogenic Nd, radiogenic Sr; Becker & Le Roex, 2006; Giuliani et al., 2015; Tappe et al., 2008) and would therefore likely decrease $^{143}Nd/^{144}Nd$ and increase $^{87}Sr/^{86}Sr$ in affected eclogites. At Lace, although LREE-enriched samples nearly span the whole range of initial $^{143}Nd/^{144}Nd$, a broad trend toward less radiogenic Nd with increasing Cr abundances is recognized, the lowest initial value, in pyroxenites, being below that of the host orangeite (Figure 6b). This may indicate that pyroxenitization preceded Cretaceous orangeite magmatism and involved an agent sampling an aged lithospheric mantle metasome, as suggested also for Orapa. At Koidu, metasomatism by a kimberlite-like melt is associated with an increase of $^{87}Sr/^{86}Sr$ in clinopyroxene and convergence to a common value of ~0.7035, clearly linked to low Li abundances, while initial $^{143}Nd/^{144}Nd$ in garnet decreases from radiogenic values (>0.5145) to a relatively constant value of ~0.5130 (Figure 6c), associated with high Cr contents. At Orapa, strongly radiogenic Sr, indicative of a metasomatic agent derived from an isotopically aged lithospheric mantle reservoir with $^{87}Sr/^{86}Sr > 0.7060$ and similar to orangeites (Becker & Le Roex, 2006), is mostly associated with LREE-enriched eclogites (Figure 6a). In contrast, in eclogites from the northern Slave craton, the metasomatic agent had less radiogenic Sr, whereas in the central Slave craton a link between LREE-enrichment and $^{87}Sr/^{86}Sr$ is not evident. Conversely, the preservation of unradiogenic Sr in the eclogite suite from the Victor kimberlite, Superior craton, was suggested to indicate negligible effects of such metasomatism (Smit et al., 2014).

5.1.6. Depth, Extent, and Timing of UM Carbonated Melt Metasomatism

The nature and intensity of metasomatism vary with depth and may be localized due to differences in the density of fluids vs. melts allowing the former to rise to shallower depths (Griffin et al., 2003). Further

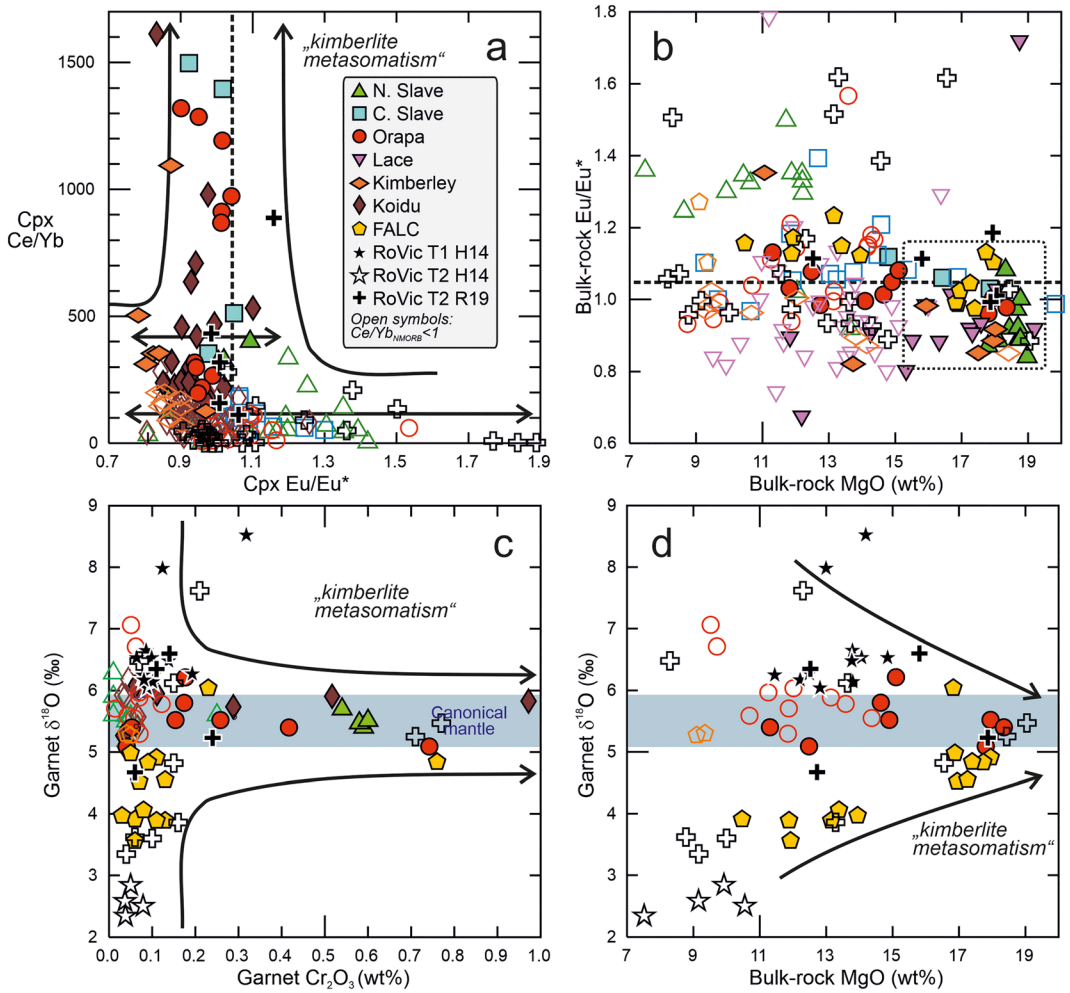

Figure 5. Muting of crustal signatures in LREE-enriched eclogites, ascribed to interaction with a UM carbonated melt similar to kimberlite ("kimberlite metasomatism"). Crustal signatures are gauged as (a,b) Eu/Eu* (chondrite-normalized Eu/(Sm*Gd)^0.5; chondrite of Sun & McDonough, 1989) and (c,d) $\delta^{18}O$ (‰) in garnet reflecting crustal differentiation and seawater alteration in low-pressure protoliths, respectively, whereas metasomatic intensity is gauged with Ce/Yb, Cr_2O_3 (wt%), and MgO (wt%). The range of Eu/Eu* and $\delta^{18}O$ is larger in unenriched than in LREE-enriched eclogites. Canonical mantle $\delta^{18}O$ range from Mattey et al. (1994). Filled symbols are for LREE-enriched samples (NMORB-normalized Ce/Yb >1; NMORB from Gale et al., 2013) and open symbols for unenriched samples, except Kimberley where open symbols show samples enriched in both LREE and HREE. References as in Figure 1, plus Czas et al. (2018) for samples from Fort a la Corne (Sask craton), Huang et al. (2012, 2014) for Type I and Type II eclogites, and Radu et al. (2019) for Type II eclogites from Roberts Victor (Kaapvaal).

effects are related to the solidus of the metasomatized lithology: harzburgites with high solidi are more likely to be percolated by fluids whereas lherzolites and eclogites with lower solidi may be percolated more readily by melts (Stachel & Luth, 2015). Keeping the uncertainties outlined in chapter 3 in mind, the LREE-enrichment in eclogites from Orapa, Diavik, northern Slave, and Kimberley is focused at midlithospheric depths corresponding to ~2–5 GPa (Figures 7a and 7b). This is similar to the depths where continental midlithospheric discontinuities are recorded, which have been ascribed to the accumulation of metasomatic minerals, such as phlogopite and carbonate, which are directly (xenoliths) or indirectly (via their contribution to mantle magmas) observed in cratons (Aulbach, Massuyeau, et al., 2017; Rader et al., 2015). The inferred silicate melt metasomatism causing HREE-enrichment in Kimberley eclogites is largely restricted to higher pressures of ~4-5 GPa (Figure 7c), closer to where intense melt percolation and refertilization of the peridotitic lithosphere are observed (e.g., O'Reilly & Griffin, 2013), and is rare to absent in the other eclogite suites considered here. In the Sask craton, LREE-enrichment in eclogites, unaccompanied by HREE addition, occurs at similar pressures (Figure 7d). Nevertheless, in common with

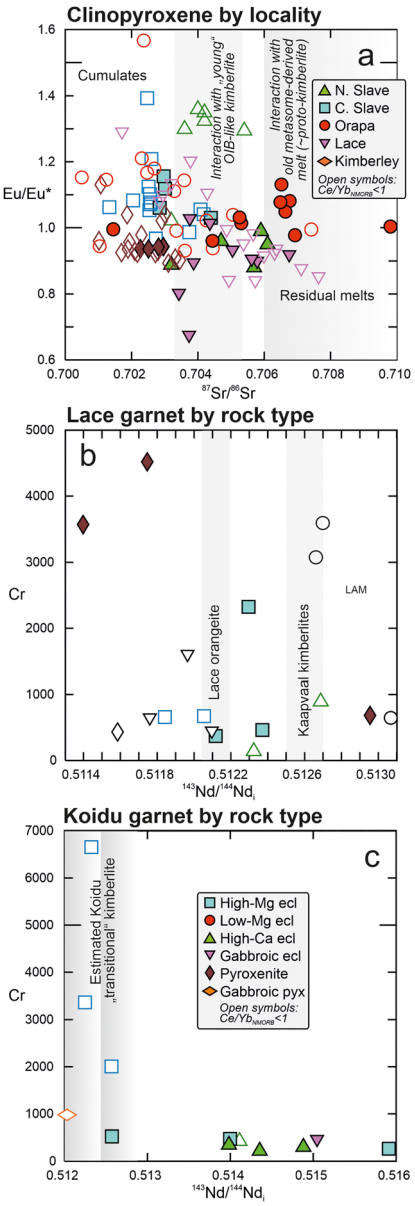

Figure 6. (a) Eu/Eu* (chondrite-normalized Eu/(Sm*Gd)^0.5; CI chondrite of Sun & McDonough, 1989) as a function of $^{87}Sr/^{86}Sr$ in clinopyroxene from various localities; for samples with variable $^{87}Sr/^{86}Sr$ from Orapa, the lowest value is shown, with the assumption that the least radiogenic value represents the least compromised one with respect to later metasomatism. Eclogites with gabbroic (cumulate) protoliths are expected to have higher Eu/Eu* than those with protoliths originating as residual melts, and to evolve to lower and higher $^{87}Sr/^{86}Sr$, respectively. Depending on this pre-history, metasomatism by young asthenosphere-derived kimberlites, and by orangeites having an aged lithospheric metasome component, may increase or decrease the original $^{87}Sr/^{86}Sr$. Cr content (ppm) in garnet, as a measure of metasomatic intensity, as a function of initial Nd isotopic composition ($^{143}Nd/^{144}Nd_i$) in eclogites from (b) Lace (this work) and (c) Koidu (Aulbach, Höfer, & Gerdes, 2019). Shown for comparison is range of $^{143}Nd/^{144}Nd_i$ of the Lace orangeite (Howarth et al., 2011) and of Kaapvaal kimberlites (sensu stricto; Le Roex et al., 2003). The $^{143}Nd/^{144}Nd$ of the compositionally transitional Koidu kimberlite is possibly approximated, but possibly approximated by the unradiogenic Nd recorded in garnet from metasomatized high-Mg eclogite.

HREE-enriched Kimberley eclogites, Sask samples are conspicuously Nb-enriched, whereas in the northern Slave craton, this enrichment is restricted to a very narrow pressure interval (Figure 7d).

Bearing in mind that the number of samples is probably too low for statistical significance, the proportion of pristine vs. metasomatized eclogite in each of the suites (as gauged by bulk-rock $Ce/Yb_N > 1$) may be used to assess the extent of UM carbonated melt metasomatism. This indicates that between ~20% (Lace, Diavik) and ~40% (northern Slave, Orapa) of the eclogite reservoir was affected by UM carbonated melt metasomatism (Table 1). The observation that ascending kimberlites do not sample the mantle lithosphere in a representative manner (Moss et al., 2018) adds further uncertainty to this estimate.

As is true for their peridotitic counterparts (e.g., Griffin, Shee, et al., 1999; Jollands et al., 2018), LREE enrichment in some eclogites appears to be temporally related to kimberlite-like magmatism (though not directly caused by the host kimberlite). This is evidenced by diamond brecciation and elemental heterogeneity in deeply derived eclogites from the Sask craton, which occurred immediately prior to entrainment, as modeled from diffusion profiles (Czas et al., 2018). In the absence of such heterogeneity and given that zircon formation is related to auto-metasomatism during emplacement of oceanic crust (as discussed above), the timing of mantle metasomatic effects in LREE-enriched eclogites is difficult to pin down precisely due to their multistage evolution. Some metasomatism is plausibly related to reactivation of older metasomes related to lamproite magmatism (Mitchell, 2006) and failed protokimberlite magmatism (e.g., Giuliani et al., 2014). This is the case for Koidu, where Sr-Nd isotopes in eclogites indicate a Neoproterozoic age for metasomatism, possibly due to extension during Rodinia break-up (Aulbach, Höfer, & Gerdes, 2019). Southern Africa presents a special case because older lamproite/orangeite magmatism (>110 Ma) was superseded by kimberlite magmatism sensu stricto (mostly ≤95 Ma), accompanied by strong metasomatism, warming and loss of the deepest part of the lithospheric root (Griffin et al., 2003; Kobussen et al., 2009). As outlined above, eclogites from the older Lace kimberlite are only mildly overprinted (20% affected), whereas higher proportions have been affected at Orapa and Kimberley, plausibly between 110 and 95 Ma. Circumstantial evidence for a young event at Lace (relative to host orangeite emplacement) comes from the inverse relationship of initial $^{143}Nd/^{144}Nd$ with Sm/Nd in metasomatic pyroxenites (not shown), which cannot persist for extended periods of time, as radiogenic ingrowth would cause a counterclockwise rotation of the relationship. At Orapa, several samples show significant Sr isotopic heterogeneity (Table S7), e.g., from 0.7010 to 0.7043 in diamondiferous eclogite 801; low measured Rb/Sr excludes ablation of kimberlite-contaminated areas as the origin of this variability. This variability also qualitatively suggests relatively recent metasomatic overprint, with insufficient time and/or heat to allow rehomogenization. Of note, a phlogopite-rich eclogite (30 vol%) occurs in the ca. 1150 Ma Premier (Cullinan) kimberlite (Dludla et al., 2006). The age of this kimberlite is similar to the age determined by Ar-Ar dating on metasomatically introduced phlogopite in peridotite xenoliths from various Kaapvaal kimberlites (Hopp et al., 2008). This provides *bona fide* evidence that significant hydration in the Kaapvaal craton is not a phenomenon restricted to relatively recent deep protokimberlite activity, and circumstantial evidence

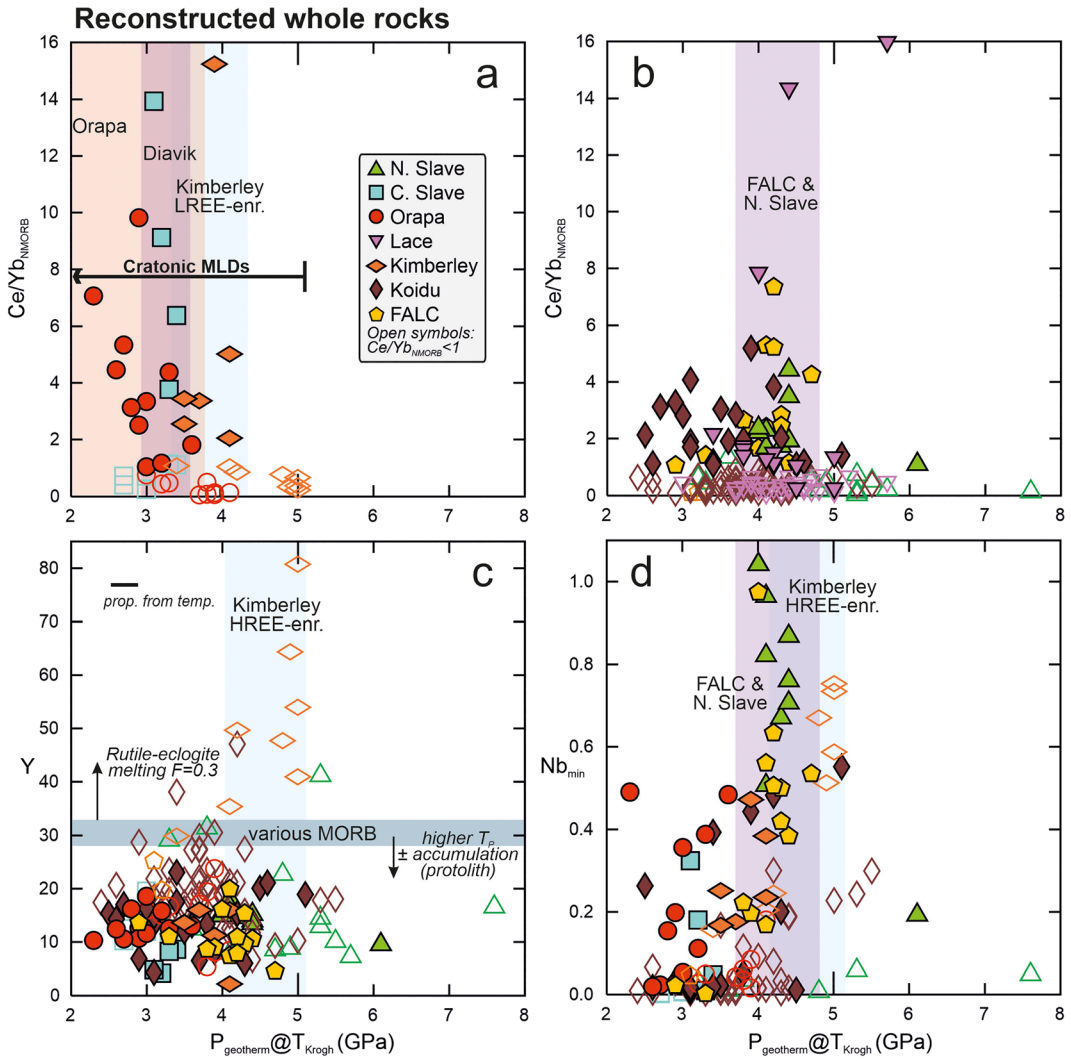

Figure 7. Depth focusing of metasomatism with LREE-enrichment ("LREE-enr.") and with both LREE- and HREE-enrichement ("HREE-enr.") gauged by (a,b) NMORB-normalized Ce/Yb (NMORB of Gale et al., 2013), (c) Y (ppm), and (d) Nb (ppm) in reconstructed whole rocks as a function of pressure (GPa) obtained by iterative solution of temperature (Krogh, 1988) with the regional geotherm (see section 3 and text S1), as parameterized from Hasterok and Chapman (2011). Pressure range of cratonic midlithospheric discontinuities (MLDs) in (a) from Rader et al. (2015). As applies to all incompatible elements (with varying sensitivity), Y contents decrease with increasing mantle potential temperature (T_P) and melt fraction during melt generation in the protolith stage and are excluded during accumulation, whereas they increase with increasing degree of igneous differentiation of the crustal protoliths. Partial melting upon subduction, modeled as melt extraction from rutile eclogite with a melt fraction F of 0.3, increases Y (see also Figure S3); estimates for various NMORB from Sun and McDonough (1989) and Gale et al. (2013). Nb contents are minimum because rutile, a frequent accessory mineral in eclogites known to control Nb abundances, has not been considered in bulk rock reconstruction (see text for details). Uncertainty on the pressure along a 38 mW/m^2 geothermal gradient is 0.38 GPa propagated for a 60 °C uncertainty at a temperature of 1000 °C ("prop. from temp."). Filled symbols are for LREE-enriched samples (NMORB-normalized Ce/Yb >1) and open symbols for unenriched samples, except Kimberley where open symbols show samples enriched in both LREE and HREE. References as in Figure 1.

that phlogopite addition precursory to kimberlite magmatism is a recurrent process since at least the Mesoproterozoic.

5.2. Effects of Mantle Metasomatism on Eclogite Physical Properties

In order to assess the effects of mantle metasomatism on density and shear-wave velocity of mantle eclogites, we used the same methods as in Garber et al. (2018) (cf.Connolly, 2009; Stixrude &Lithgow-Bertelloni, 2005, 2011), with the difference that we (1) used measured rather than calculated

mineral compositions; (2) did not consider accessory phases, such as coesite or kyanite (which due to their low abundance are not necessarily exposed at thin section scale); (3) used pressure-temperature estimates obtained by iterative solution of temperatures derived from the garnet-clinopyroxene Mg-Fe exchange thermometer of Krogh (1988) with regional peridotite-derived geotherms, as parameterized from Hasterok and Chapman (2011); and (4) applied mineral modes of 45% clinopyroxene and 55% garnet, compared to ~40–45% and ~55–60%, respectively, employed in Garber et al. (2018), the effect of which is explored in Figure S5. Briefly, the molar volume, density, and shear moduli of each relevant clinopyroxene and garnet compositional endmember were calculated over a large pressure-temperature grid in Perple_X (using the elastic parameters and equations of state in Stixrude & Lithgow-Bertelloni, 2005, 2011), followed by extraction of the relevant endmember data from the grid at the pressure and temperature of each xenolith using MATLAB. Clinopyroxene and garnet endmember proportions were calculated directly from EPMA major-element oxide data, with clinopyroxene site assignation and endmember inversion performed using the methods of Morimoto et al. (1988) and Dietrich and Petrakakis (1986), respectively. Fe^{3+} and Cr contents are relatively minor across the sample suite, thus these endmembers were not considered, nor would they significantly affect the results if they were included (cf. discussion in Garber et al., 2018). Molar volumes and densities were calculated for clinopyroxene and garnet using Voigt averages of their compositional endmember properties, whereas shear moduli (Gs) were calculated for the same phases with molar-volume weighted Reuss averages of endmember shear moduli (cf. Stixrude & Lithgow-Bertelloni, 2005, equations (9)–(11)). Finally, bulk-rock densities were calculated using Voigt averages of the solid-solution densities; these densities were then used in combination with Voigt-Reuss-Hill averaged bulk-rock shear moduli to calculate shear-wave velocities. Seismic attenuation was not considered, and thus calculated shear-wave velocities are maxima. Electrical conductivity was calculated using Hashin-Shtrikman lower (HS−) and upper (HS+) bounds based on formulations in Jones et al. (2009) and using the pressure-temperature-conductivity relationship for dry garnet in Dai and Karato (2009) and the temperature-H_2O-conductivity relationship for wet clinopyroxene in Zhao and Yoshino (2016).

5.2.1. Density

One of the most conspicuous effects of UM carbonated melt metasomatism is FeO dilution (Figure 3d), with a corresponding decrease in the almandine and hedenbergite endmembers. Hence, the density of metasomatized eclogites is systematically lower than unmetasomatized eclogites from the same locality (Figures 8a and 8b; Table 1). The calculated densities for LREE-enriched eclogites are maxima if bulk rocks have clinopyroxene-garnet modes closer to 50:50 than to the 45:55 employed, as discussed above. Despite this reduction, densities of metasomatized eclogites are still considerably higher than those of peridotites at similar depths, which are restricted to <3.5 g/cm^3 even for the maximum bound determined for cold cratonic peridotite by Garber et al. (2018) (i.e., using the same methods as in this study). Kopylova et al. (2004) report lower densities for mantle eclogite xenoliths from the northern Slave craton based on laboratory-determined derivatives for eclogite bulk rocks (~3.4–3.5 g/cm^3; see comparison in Figure S5), but these rocks may have been affected by late-stage changes in the xenoliths (partial melting of clinopyroxene due to decompression and chemical interaction with host kimberlite; Gao et al., 2000; Pan et al., 2018). Apart from metasomatic effects, several regional peculiarities emerge. For example, even unenriched eclogites from Lace and Diavik are relatively FeO-poor and therefore have densities much lower than the average eclogite at 38 or 40 mW/m^2 from Garber et al. (2018) (Figures 8a and 8b). Conversely, unenriched eclogites from the northern Slave craton, and most eclogites from Koidu regardless of their enrichment, are more FeO-rich and hence more dense. Even recognizing these metasomatic and regional differences, the range of eclogite densities calculated in this study scatters about the range calculated by Garber et al. (2018) using thermodynamic minimization techniques along a similar geotherm.

It is worth highlighting that, since mantle metasomatism occurs after emplacement of oceanic crust into the lithospheric mantle, the density changes described above do not pertain to eclogite deeply recycled into the convective mantle. In contrast, "auto-metasomatized" eclogite, which interacted with pelite-derived melts in subduction mélanges, also is markedly FeO-poor (Figure 3d), hence less dense. Such interactions may decrease slab pull and also be a factor causing slabs to stagnate at midmantle depths (Xu et al., 2019), as the density difference with the dominant mantle consisting of pyrolite is much smaller for low-Fe than for high-Fe eclogite, although the extent of this type of metasomatism is difficult to assess.

5.2.2. Shearwave Velocity (V_S)

At constant composition and pressures ~3 to 3.5 GPa kyanite disappears and eclogite assemblages become dominated by garnet and clinopyroxene, with phase compositions and modal proportions depending on bulk-rock eclogite composition. At higher pressures, eclogite V_S decreases along the geotherm as temperature increases, and is lower for warm than for cold conductive geotherms (e.g., Garber et al., 2018). Shear-wave velocity is also sensitive to composition as it increases with decreasing hedenbergite and almandine component (cf. Garber et al., 2018, their Figure 6), which are lowered by UM carbonated melt metasomatism, and increases weakly with bulk-rock SiO_2 content, which is higher in many LREE-enriched eclogites inferred to have experienced stealth clinopyroxene addition (Figure 3c). However, because metasomatism serves to deplete *both* the seismically slowest endmembers (hedenbergite and almandine) and the seismically fastest endmembers (jadeite and grossular), metasomatized eclogite V_S is typically similar to velocities calculated for unmetasomatized eclogites from the same region (Figures 8c and 8d). As for density, there are distinct regional differences in eclogite V_S: eclogites from Lace are seismically fast (≥4.8 km/s) regardless of enrichment, as are unenriched eclogites from Diavik at pressures >5 GPa, which may be explained by the generally SiO_2-rich and FeO-poor compositions of these suites (Figures 3c and 3d). Eclogites from the northern Slave craton, presumably equilibrated to a cold conductive geotherm, give some of the highest V_S at midcratonic lithosphere depth (Figure 8d). Notably, with the exception of the Lace and N. Slave eclogite suites, and even allowing for a small model-dependent uncertainty in V_S (≤0.02 km/s; Garber et al., 2018), most eclogite samples in this study are seismically slower than the range of eclogite compositions considered in Garber et al. (2018). Such differences arise from a slight discrepancy between clinopyroxene and garnet compositional endmembers calculated thermodynamically (Garber et al., 2018) relative to those observed in mantle eclogites (this study), but a more significant effect arises from differences in the calculated modes of each phase between studies (Figure S5)—particularly because eclogite bulk compositions do not deviate significantly between the two different approaches.

5.2.3. Electrical Conductivity

Electrical conductivity, which can be extracted from regional magnetotelluric studies, is strongly temperature-dependent, but also increases with increasing mineral H_2O content (e.g., Jones et al., 2009; Yang et al., 2011; Zhao & Yoshino, 2016). With the exception of the Roberts Victor and Udachnaya (Siberia) eclogites studied by Huang et al. (2014) and Kolesnichenko et al. (2018), respectively, there are no comprehensive published studies on H_2O content in mantle eclogite suites. Garnet in both studies has very low H_2O contents, but whereas clinopyroxene in eclogite from Udachnaya has a low median content of ~40 ppm, that from Roberts Victor contains ~760 ppm H_2O. Although the relationship between metasomatism and H_2O content in peridotitic minerals is tenuous at best (Marshall et al., 2018), we calculate H_2O content in clinopyroxene from LREE-enriched and HREE-enriched eclogites assuming equilibrium with a melt containing 3 wt% H_2O (similar to estimates for primitive southern African kimberlites and orangeites), whereas 100 ppm is assigned to clinopyroxene from unenriched eclogites. A comparison of expected H_2O concentrations using the approach outlined above vs. measured concentrations in eclogites from Roberts Victor (Huang et al., 2014) shows that, unsurprisingly, there is only a very crude correspondence, though median values do not differ strongly (760 ppm measured vs. 620 ppm calculated). Combined with dry garnet, we obtain bulk eclogite conductivities as outlined in the caption to Figure 8. Our aim is to obtain a sense of the importance of this parameter to bulk eclogitic electrical conductivity. For these hypothetical H_2O contents, LREE-enriched eclogites have predictably higher conductivities than unenriched eclogites at a given depth (hence, temperature). As hypothetical H_2O abundances were calculated for both LREE- and HREE-enriched eclogites from Kimberley, they plot along a single trend (Figures 8e and 8f). Conductivities are higher than those expected for average eclogite used in Garber et al. (2018) along applicable geotherms (36 mW/m^2 for the northern Slave craton; 38 mW/m^2 for Lace, Roberts Victor, Diavik, and Koidu; 40 mW/m^2 for Kimberley), which directly reflects their choice of purely dry assemblages.

6. Implications and Conclusions

The role of mantle eclogite in the density, seismic velocity, and electrical conductivity signatures of cratonic lithosphere has recently been highlighted, using average eclogite and peridotite compositions as well as high-Mg and low-Mg extremes with depth (Garber et al., 2018). The present study aims to shed more light

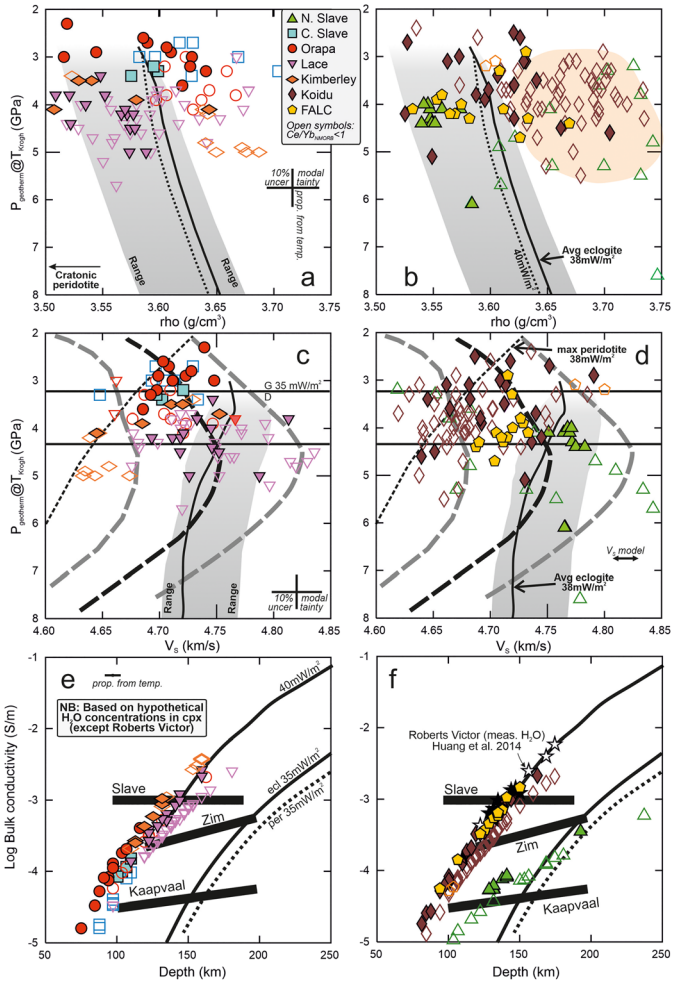

Figure 8. Variation of (a, b) density (rho, g/cm^3), (c, d) shearwave velocity (V_S, km/s), and (e, f) hypothetical (average of upper and lower bound) bulk electrical conductivity (S/m) with pressure (GPa) or depth (km) in eclogites; suites have been split into two panels for clarity. Density and shear-wave velocity were calculated for eclogite mineral endmember proportions weighted by modes using the same methods and data as in Garber et al. (2018) (cf.Connolly, 2009 ; Stixrude & Lithgow-Bertelloni, 2005, 2011), but at 5% lower garnet modes, 5% higher clinopyroxene modes, and at pressure-temperature estimates obtained as outlined in the text. Electrical conductivity was calculated based on formulations in Jones et al. (2009), Dai and Karato (2009), and Zhao and Yoshino (2016) (see text for further details). To illustrate the effect of water and in accord with rare observational data from eclogites (Huang et al., 2014), it is assumed that all garnet is dry and that clinopyroxene in LREE-enriched eclogites, and in HREE-enriched eclogites from Kimberley, has equilibrated with a kimberlite-like melt containing 3 wt% H_2O, whereas clinopyroxene in unenriched eclogites was assumed to contain 100 ppm H_2O. The distribution coefficient $^{\text{clinopyroxene/melt}}D_H$ depends on Al_2O_3 in clinopyroxene and was calculated using the relationship reported in Aubaud et al. (2008). Conductivities are hypothetical values except for eclogites from Roberts Victor where it was calculated for measured H_2O contents in clinopyroxene. Shown for comparison in (a)–(d) are results for average eclogite as well as low-Mg and high-Mg extremes from Garber et al. (2018) for 38 mW/m^2 as interpolated from their results for 35 and 40 mW/m^2. In panels (c) and (d) the average and bounds of average cratonic V_S in the model of French and Romanowicz (2014) is shown with black and gray long stipples, respectively, and graphite-diamond (G-D) boundary for a geotherm of 35 mW/m2 (indicated) and 40 mW/m2 (line below) is based on Day (2012). Uncertainties related to a 10% modal variation (0.45 gt plus 0.55 clinopyroxene, as opposed to the 0.55 gt plus 0.45 clinopyroxene used in bulk rock reconstruction) are shown as error bars. Uncertainty on the pressure along a 38 mW/m^2 geothermal gradient is 0.38 GPa propagated for a 60 °C uncertainty at a temperature of 1000 °C ("prop. from temp."). Model-dependent differences between V_S are ≤0.02 km/s (Garber et al., 2018). Solid and stippled black lines in (e) and (f) are conductivities calculated by Garber et al. (2018) for average eclogite and peridotite, respectively, for conductive geotherms corresponding to a surface heat flow of 35 (lower conductivity) and 40 mW/m^2 (higher conductivity); black bars are conductivities extracted from magnetotelluric studies in the Slave, Zimbabwe (Zim), and Kaapvaal cratons as reported in Garber et al. (2018). The uncertainty arising from a 10% modal variation is not discernible at the scale displayed. Filled symbols are for LREE-enriched samples (NMORB-normalized Ce/Yb >1; NMORB from Gale et al., 2013) and open symbols for unenriched samples, except Kimberley where open symbols show samples enriched in both LREE and HREE. References as in Figure 1, plus Huang et al. (2014) for samples from Roberts Victor and Czas et al. (2018) for samples from Fort a la Corne (Sask craton).

on the physical properties of mantle eclogite, and also the effect of UM carbonated melt- and auto-metasomatism on eclogite composition, using a wide range of observed mantle eclogite compositions and their distribution with depth for various cratons.

The regional extent of mantle metasomatism remains poorly constrained. On the one hand, it has frequently been cautioned that the mantle sampled by kimberlites is anomalous because magmatism occurs along, in cases multiply, reactivated lithospheric pathways (e.g., Afonso et al., 2008). Consistent with this, the positive buoyancy observed in cratonic areas away from kimberlite provinces, as opposed to near-neutral buoyancy within these areas, has been ascribed to anomalous lithosphere enrichment associated with kimberlite magmatism, indicating the presence of more refractory mantle away from those regions (Artemieva et al., 2019). On the other hand, cratonic midlithospheric discontinuities, ascribed to deposition of metasomes (e.g., Rader et al., 2015), are not restricted to kimberlite provinces and suggest that metasomatism widely affects deep and warm lithospheric keels underlying cold and viscous cratonic cores (e.g., Aulbach, Massuyeau, & Gaillard, 2017). Regardless of the extent of metasomatism, eclogite emplacement into the cratonic mantle starting in Mesoarchaean to Palaeoproterozoic time (Shirey & Richardson, 2011) relates to large-scale geodynamic processes and is unrelated to areas of kimberlite magmatism where subduction relics are accidentally exhumed as xenoliths. In addition to uncertainties regarding regional extent, there are also questions regarding the relevance to present-day geophysical observations. Thus, although the effects of older metasomatism may persist through time (e.g., isotopically aged, ancient metasomes tapped during Phanerozoic lamproite magmatism; Mitchell, 2006), all xenoliths provide a snapshot of lithospheric conditions at the time of entrainment in the host kimberlite, in cases several 100 Ma ago, and subsequent events may have modified the lithosphere up until the present. This is exemplified in the southern African case, where significant warming, refertilization, and thinning occurred between older (~Jurassic) orangeite and younger (~Cretaceous) kimberlite emplacement (e.g., Kobussen et al., 2009).

If the metasomatism identified in the various eclogite suites under consideration here is geographically restricted, it implies that (1) in areas of kimberlite activity, metasomatic densification of mantle peridotite (e.g., Lee et al., 2011) may be partially offset by the lowered density of metasomatized eclogite, and (2) in areas away from kimberlite activity, positive/excess buoyancy of low-density refractory peridotite (Poudjom Djomani et al., 2001) may be balanced by the presence of dense (i.e., unmetasomatized) eclogite, as suggested by Kelly et al. (2003) and Garber et al. (2018). Except in HREE-enriched Kimberley eclogites, where high FeO contents at higher pressures reflect infiltration of asthenosphere-derived silicate melt, there is no correlation of FeO with temperature, suggesting that no density sorting has taken place within the lithosphere. Very dense eclogites at Koidu and Diavik persist between ~2.5 and 5.5 GPa (Figure 8b), possibly attesting to the strength, buoyancy, and high viscosity of the dominant peridotitic lithosphere.

Although Kopylova et al. (2016) conclude that eclogites from the Slave craton do not derive from depths corresponding to geophysically detected discontinuities, the concentration of seismically fast, LREE-enriched, SiO_2-rich, and FeO-poor eclogites at midlithospheric depths at several localities may help explain the high maximum velocities observed at similar depths in the shearwave tomographic model of French and Romanowicz (2014) (Figures 8c and 8d). However, the results presented here also complicate interpretations that significant eclogite fractions may help explain the fast shear-wave velocity signature of cratonic mantle lithosphere globally (e.g., Garber et al., 2018). On the one hand, the decreased density but unmodified V_S signature of metasomatized eclogite permits significant fractions of chemically modified, stiff, and fast-V_S eclogite to be hosted in cratonic lithosphere—perhaps far more than postulated using gravity and density limitations (≤20 vol%; Garber et al., 2018). On the other hand, even this theoretical limit exceeds those from empirical studies, e.g., those using surveys of garnet xenocrysts (4%; McLean et al., 2007) or those based on thermal state and heat production constraints (0.17% to 1.5%; Russell et al., 2001). Further, though there are particular suites with Vs significantly higher than the cratonic average (Figure 8; cf. French & Romanowicz, 2014), most calculated eclogite shear-wave velocities in this study are slower than velocities calculated for thermodynamically modeled eclogites, reflecting a key difference in the modal proportions of clinopyroxene and garnet. Therefore, though small fractions of either metasomatized or unmetasomatized eclogite increase the bulk shear-wave velocity of cratonic lithosphere above that of peridotite alone, our results emphasize that such contributions cannot reconcile the observed V_S; assuming that xenolith *P-T* conditions accurately represent craton thermal structures, other constituents with fast shear-wave velocities (e.g., diamond) must be present. Notably, we have not considered diamond in concert with our eclogite results, but recognize the potential for V_S modifications driven by either diamond growth or destruction during metasomatism. Any diamond in unenriched eclogites, and diamond in the extremely diamond-rich

LREE-enriched eclogites from the northern Slave craton (Smart et al., 2009) will increase bulk eclogite V_S and decrease the fraction of eclogite in explaining bulk mantle V_S.

Eclogite conductivity is much more temperature-dependent, hence also dependent on the geothermal gradient in addition to the depth of xenolith derivation, than on degree of hydration. Nevertheless, hypothetical enrichment in H_2O may have occurred along with LREE around the depths of cratonic midlithospheric discontinuities, focused at ~60 to 160 km and potentially linked to the formation of amphibole-/phlogopite- and carbonate-bearing metasomes (Aulbach, Massuyeau, & Gaillard, 2017; Rader et al., 2015). Concentrations of H_2O-rich eclogite have been suggested to cause conductivity anomalies in the upper mantle (Liu et al., 2019) and may help explain anomalous conductivities observed in the Slave cratonic midlithosphere (Jones et al., 2001) and elsewhere (Selway, 2014). If H_2O enrichment occurred along with LREE around the depths of cratonic midlithospheric discontinuities as observed in several localities (Diavik, Orapa, Kimberley), it may establish a link to the formation of amphibole-/phlogopite- and carbonate-bearing metasomes, which have been suspected of acting as weak zones where future decratonization may occur (Aulbach, Massuyeau, & Gaillard, 2017; Rader et al., 2015). Perhaps not coincidentally, olivine in peridotite xenoliths from the Kaapvaal craton reaches a maximum H_2O content at ~160 km depth (Baptiste et al., 2012), and upward increasing intensity of hydrous metasomatism has been implicated in generating cratonic seismic velocity profiles as well as MLDs (Eeken et al., 2018). However, the conductivities of dry or hypothetical wet eclogites in this study are much higher than bulk conductivities reported for the Kaapvaal cratonic lithosphere, suggesting that either eclogites are generally much drier than inferred here and/or placing limits on the proportion of eclogite that may be present in the regional lithospheric mantle.

Acknowledgments

Discussions with Yana Fedortchouk are greatly appreciated. Jens Fiebig is thanked for access to the stable isotope laboratory, and Dominik Gudelius for carrying out the analyses. We gratefully acknowledge reviews by Thomas Stachel and Maya Kopylova, as well as editorial comments by Ulrich Faul, all of which significantly improved the manuscript. Funding to SA by the Deutsche Forschungsgemeinschaft under DFG-grant AU356/10 is greatly appreciated. FIERCE is financially supported by the Wilhelm and Else Heraeus Foundation and by the Deutsche Forschungsgemeinschaft (DFG, INST 161/921-1 FUGG and INST 161/923-1 FUGG), which is gratefully acknowledged. This is FIERCE contribution No. 14. KSV and MM acknowledge financial support from the SA Department of Science and Technology (DST) through their Research Chairs initiative, as administered by the National Research Foundation (NRF), as well as financial support from the Centre of Excellence for Integrated Mineral and Energy Resource Analysis (CIMERA) at the University of Johannesburg. JMG acknowledges financial support from National Science Foundation grant OISE-1545903 and Penn State University. The authors declare no conflicts of interest. Geochemical data are available at IEDA online database (https://doi.org/10.1594/IEDA/111491).

Open access funding enabled and organized by Projekt DEAL.

References

Adam, J., & Green, T. (2006). Trace element partitioning between mica- and amphibole-bearing garnet lherzolite and hydrous basanitic melt: 1. Experimental results and the investigation of controls on partitioning behaviour. *Contributions to Mineralogy and Petrology*, *152*(1), 1–17. https://doi.org/10.1007/s00410-006-0085-4

Afonso, J. C., Fernandez, M., Ranalli, G., Griffin, W. L., & Connolly, J. A. D. (2008). Integrated geophysical-petrological modeling of the lithosphere and sublithospheric upper mantle: Methodology and applications. *Geochemistry Geophysics Geosystems*, *9*(5), Q05008. https://doi.org/10.1029/2007gc001834

Agashev, A. M., Pokhilenko, L. N., Pokhilenko, N. P., & Shchukina, E. V. (2018). Geochemistry of eclogite xenoliths from the Udachnaya Kimberlite Pipe: Section of ancient oceanic crust sampled. *Lithos*, *314-315*, 187–200. https://doi.org/10.1016/j.lithos.2018.05.027

Allsopp, H. L., Bristow, J. W., Smith, C. B., Brown, R., Gleadow, A. J. W., Kramers, J. D., & Garvie, O. G. (1989). A summary of radiometric dating methods applicable to kimberlites and related rocks. In J. Ross, A. L. Jacques, J. Ferguson, D. H. Green, S. Y. O'Reilly, R. V. Danchin, & A. J. A. Janse (Eds.), *Kimberlites and Related Rocks: Their Composition, Occurrence, Origin and Emplacement* (pp. 343–357). Oxford: Geological Society of Australia Special Publication. Blackwell Scientific.

Artemieva, I. M., Thybo, H., & Cherepanova, Y. (2019). Isopycnicity of cratonic mantle restricted to kimberlite provinces. *Earth and Planetary Science Letters*, *505*, 13–19. https://doi.org/10.1016/j.epsl.2018.09.034

Aubaud, C., Hirschmann, M. M., Withers, A. C., & Hervig, R. L. (2008). Hydrogen partitioning between melt, clinopyroxene, and garnet at 3 GPa in a hydrous MORB with 6 wt.% H_2O. *Contributions to Mineralogy and Petrology*, *156*(5), 607–625. https://doi.org/10.1007/s00410-008-0304-2

Aulbach, S., Creaser, R. A., Pearson, N. J., Simonetti, S. S., Heaman, L. M., Griffin, W. L., & Stachel, T. (2009). Sulfide and whole rock Re-Os systematics of eclogite and pyroxenite xenoliths from the Slave Craton, Canada. *Earth and Planetary Science Letters*, *283*(1-4), 48–58. https://doi.org/10.1016/j.epsl.2009.03.023

Aulbach, S., Gerdes, A., & Viljoen, K. S. (2016). Formation of diamondiferous kyanite-eclogite in a subduction melange. *Geochimica Et Cosmochimica Acta*, *179*, 156–176. https://doi.org/10.1016/j.gca.2016.01.038

Aulbach, S., Heaman, L. M., Jacob, D. E., & Viljoen, K. S. (2019). Ages and sources of mantle eclogites: ID-TIMS and in situ MC-ICPMS Pb-Sr isotope systematics of clinopyroxene. *Chemical Geology*, *503*, 15–28. https://doi.org/10.1016/j.chemgeo.2018.10.007

Aulbach, S., Höfer, H. E., & Gerdes, A. (2019). High-Mg mantle eclogites from Koidu (West African craton): Neoproterozoic ultramafic melt metasomatism of subducted Archaean plateau-like oceanic crust. *Journal of Petrology*, *60*(4), 723–754. https://doi.org/10.1093/petrology/egz011

Aulbach, S., & Jacob, D. E. (2016). Major- and trace-elements in cratonic mantle eclogites and pyroxenites reveal heterogeneous sources and metamorphic processing of low-pressure protoliths. *Lithos*, *262*, 586–605. https://doi.org/10.1016/j.lithos.2016.07.026

Aulbach, S., Jacob, D. E., Cartigny, P., Stern, R. A., Simonetti, S. S., Worner, G., & Viljoen, K. S. (2017). Eclogite xenoliths from Orapa: Ocean crust recycling, mantle metasomatism and carbon cycling at the western Zimbabwe craton margin. *Geochimica Et Cosmochimica Acta*, *213*, 574–592. https://doi.org/10.1016/j.gca.2017.06.038

Aulbach, S., Massuyeau, M., & Gaillard, F. (2017). Origins of cratonic mantle discontinuities: A view from petrology, geochemistry and thermodynamic models. *Lithos*, *268-271*, 364–382. https://doi.org/10.1016/j.lithos.2016.11.004

Aulbach, S., O'Reilly, S. Y., Griffin, W. L., & Pearson, N. J. (2008). Subcontinental lithospheric mantle origin of high niobium/tantalum ratios in eclogites. *Nature Geoscience*, *1*(7), 468–472. https://doi.org/10.1038/ngeo226

Aulbach, S., Stachel, T., Heaman, L. M., & Carlson, J. A. (2011). Microxenoliths from the Slave craton: Archives of diamond formation along fluid conduits. *Lithos*, *126*(3-4), 419–434. https://doi.org/10.1016/j.lithos.2011.07.012

Aulbach, S., & Viljoen, K. S. (2015). Eclogite xenoliths from the Lace kimberlite, Kaapvaal craton: From convecting mantle source to palaeo-ocean floor and back. *Earth and Planetary Science Letters*, *431*, 274–286. https://doi.org/10.1016/j.epsl.2015.08.039

Aulbach, S., Woodland, A. B., Stern, R. A., Vasilyev, P., Heaman, L. M., & Viljoen, K. S. (2019). Evidence for a dominantly reducing Archaean ambient mantle from two redox proxies, and low oxygen fugacity of deeply subducted oceanic crust. *Scientific Reports*, *9*(1), 20190. https://doi.org/10.1038/s41598-019-55743-1

Aulbach, S., Woodland, A. B., Vasilyev, P., Galvez, M. E., & Viljoen, K. S. (2017). Effects of low-pressure igneous processes and subduction on Fe^{3+}/Σ Fe and redox state of mantle eclogites from Lace (Kaapvaal craton). *Earth and Planetary Science Letters*, *474*, 283–295. https://doi.org/10.1016/j.epsl.2017.06.030

Baptiste, V., Tommasi, A., & Demouchy, S. (2012). Deformation and hydration of the lithospheric mantle beneath the Kaapvaal craton, South Africa. *Lithos*, *149*, 31–50. Barth, M. G., Rudnick, R. L., Horn, I., McDonough, W. F., Spicuzza, M. J., Valley, J. W., & Haggerty, S. E. (2001). Geochemistry of xenolithic eclogites from West Africa, Part I: A link between low MgO eclogites and Archean crust formation. *Geochimica Et Cosmochimica Acta*, *65*(9), 1499–1527. https://doi.org/10.1016/S0016-7037(00)00626-8

Barth, M. G., Rudnick, R. L., Horn, I., McDonough, W. F., Spicuzza, M. J., Valley, J. W., & Haggerty, S. E. (2002). Geochemistry of xenolithic eclogites from West Africa, part 2: Origins of the high MgO eclogites. *Geochimica Et Cosmochimica Acta*, *66*(24), 4325–4345. https://doi.org/10.1016/S0016-7037(02)01004-9

Becker, M., & Le Roex, A. P. (2006). Geochemistry of South African on- and off-craton, Group I and Group II kimberlites: Petrogenesis and source region evolution. *Journal of Petrology*, *47*(4), 673–703. https://doi.org/10.1093/petrology/egi089

Bell, D. R., Rossman, G. R., & Moore, R. O. (2004). Abundance and partitioning of OH in a high-pressure magmatic system: Megacrysts from the Monastery kimberlite, South Africa. *Journal of Petrology*, *45*(8), 1539–1564. https://doi.org/10.1093/petrology/

Beyer, C., Frost, D. J., & Miyajima, N. (2015). Experimental calibration of a garnet-clinopyroxene geobarometer for mantle eclogites. *Contributions to Mineralogy and Petrology*, *169*(2), 18. https://doi.org/10.1007/s00410-015-1113-z

Blundy, J., & Dalton, J. (2000). Experimental comparison of trace element partitioning between clinopyroxene and melt in carbonate and silicate systems, and implications for mantle metasomatism. *Contributions to Mineralogy and Petrology*, *139*(3), 356–371.

Bureau, H., Remusat, L., Esteve, M., Pinti, D. L., & Cartigny, P. (2018). The growth of lithospheric diamonds. *Science Advances*, *4*(6), eaat1602. https://doi.org/10.1126/sciadv.aat1602

Connolly, J. A. D. (2009). The geodynamic equation of state: What and how. *Geochemistry Geophysics Geosystems*, *10*, Q10014.

Creaser, R. A., Grutter, H., Carlson, J., & Crawford, B. (2004). Macrocrystal phlogopite Rb-Sr dates for the Ekati property kimberlites, Slave Province, Canada: Evidence for multiple intrusive episodes in the Paleocene and Eocene. *Lithos*, *76*(1-4), 399–414. https://doi.org/10.1016/j.lithos.2004.03.039

Czas, J., Stachel, T., Pearson, D. G., Stern, R. A., & Read, G. H. (2018). Diamond brecciation and annealing accompanying major metasomatism in eclogite xenoliths from the Sask Craton, Canada. *Mineralogy and Petrology*, *112*(S1), 311–323. https://doi.org/10.1007/s00710-018-0590-y

Dai, L. D., & Karato, S. (2009). Electrical conductivity of pyrope-rich garnet at high temperature and high pressure. *Physics of the Earth and Planetary Interiors*, *176*(1-2), 83–88. https://doi.org/10.1016/j.pepi.2009.04.002

Davis, G. L. (1977). The ages and uranium content of zircons from kimberlites and associated rocks. Paper presented at the 2nd International Kimberlite Conference, Santa Fe, USA.

Dawson, J. B. (1984). Contrasting types of upper mantle metasomatism. In J. Kornprobst (Ed.), *Kimberlites. II. The mantle and crust-mantle relationships* (pp. 289–294). Amsterdam: Elsevier.

Day, H. W. (2012). A revised diamond-graphite transition curve. *American Mineralogist*, *97*(1), 52–62.

De Stefano, A., Kopylova, M. G., Cartigny, P., & Afanasiev, V. (2009). Diamonds and eclogites of the Jericho kimberlite (Northern Canada). *Contributions to Mineralogy and Petrology*, *158*(3), 295–315.

Dietrich, H., & Petrakakis, K. (1986). A linear algebraic method for the calculation of pyroxene endmember components. *Tchermaks Mineralogische und Petrographische Mitteilungen*, *35*, 275–285.

Djomani, Y. H. P., O'Reilly, S. Y., Griffin, W. L., & Morgan, P. (2001). The density structure of subcontinental lithosphere through time. *Earth and Planetary Science Letters*, *184*(3-4), 605–621.

Dludla, S., le Roex, A. P., & Gurney, J. J. (2006). Eclogite xenoliths from the Premier kimberlite, South Africa: Geochemical evidence for a subduction origin. *South African Journal of Geology*, *109*(3), 353–368. https://doi.org/10.2113/gssajg.109.3.353

Dohmen, R., Kasemann, S. A., Coogan, L., & Chakraborty, S. (2010). Diffusion of Li in olivine. Part I: Experimental observations and a multi species diffusion model. *Geochimica Et Cosmochimica Acta*, *74*, 274–292.

Eeken, T., Goes, S., Pedersen, H. A., Arndt, N. T., & Bouilhol, P. (2018). Seismic evidence for depth-dependent metasomatism in cratons. *Earth and Planetary Science Letters*, *491*, 148–159.

Fedortchouk, Y., & Canil, D. (2004). Intensive variables in kimberlite magmas, Lac de Gras, Canada and implications for diamond survival. *Journal of Petrology*, *45*(9), 1725–1745.

Fedortchouk, Y., Liebske, C., & McCammon, C. (2019). Diamond destruction and growth during mantle metasomatism: An experimental study of diamond resorption features. *Earth and Planetary Science Letters*, *506*, 493–506. https://doi.org/10.1016/j.epsl.2018.11.025

French, S. W., & Romanowicz, B. A. (2014). Whole-mantle radially anisotropic shear velocity structure from spectral-element waveform tomography. *Geophysical Journal International*, *199*(3), 1303–1327. https://doi.org/10.1093/gji/ggu334

Gaetani, G. A., Asimow, P. D., & Stolper, E. M. (2008). A model for rutile saturation in silicate melts with applications to eclogite partial melting in subduction zones and mantle plumes. *Earth and Planetary Science Letters*, *272*(3-4), 720–729. https://doi.org/10.1016/j.epsl.2008.06.002

Gale, A., Dalton, C. A., Langmuir, C. H., Su, Y. J., & Schilling, J. G. (2013). The mean composition of ocean ridge basalts. *Geochemistry Geophysics Geosystems*, *14*(3), 489–518. https://doi.org/10.1029/2012gc004334

Gao, S., Kern, H., Liu, Y. S., Jin, S. Y., Popp, T., Jin, Z. M., et al. (2000). Measured and calculated seismic velocities and densities for granulites from xenolith occurrences and adjacent exposed lower crustal sections: A comparative study from the North China craton. *Journal of Geophysical Research-Solid Earth*, *105*(B8).

Garber, J. M., Maurya, S., Hernandez, J. A., Duncan, M. S., Zeng, L., Zhang, H. L. L., et al. (2018). Multidisciplinary constraints on the abundance of diamond and eclogite in the cratonic lithosphere. *Geochemistry Geophysics Geosystems*, *19*(7), 2062–2086. https://doi.org/10.1029/2018gc007534

Giuliani, A., Phillips, D., Kamenetsky, V. S., Kendrick, M. A., Wyatt, B. A., Goemann, K., & Hutchinson, G. (2014). Petrogenesis of mantle polymict breccias: Insights into mantle processes coeval with kimberlite magmatism. *Journal of Petrology*, *55*(4), 831–858. https://doi.org/10.1093/petrology/egu008

Giuliani, A., Phillips, D., Woodhead, J. D., Kamenetsky, V. S., Fiorentini, M. L., Maas, R., et al. (2015). Did diamond-bearing orangeites originate from MARID-veined peridotites in the lithospheric mantle? *Nature Communications*, *6*(1), 6837. https://doi.org/10.1038/ncomms7837

Gregory, R. T., & Taylor, H. P. (1981). An oxygen isotope profile in a section of cretaceous oceanic crust, Samail ophiolite, Oman: Evidence for δ18O buffering of the oceans by deep (>5 km) seawater-hydrothermal circulation at mid-ocean ridges. *Journal of Geophysical Research*, *86*(NB4), 2737–2755.

Griffin, W. L., Doyle, B. J., Ryan, C. G., Pearson, N. J., O'Reilly, S. Y., Davies, R., et al. (1999). Layered mantle lithosphere in the Lac de Gras area, Slave Craton: Composition, structure and origin. *Journal of Petrology*, *40*(5), 705–727. https://doi.org/10.1093/petroj/40.5.705

Griffin, W. L., O'Reilly, S. Y., Natapov, L. M., & Ryan, C. G. (2003). The evolution of lithospheric mantle beneath the Kalahari Craton and its margins. *Lithos*, *71*(2-4), 215–241. https://doi.org/10.1016/j.lithos.2003.07.006

Griffin, W. L., Shee, S. R., Ryan, C. G., Win, T. T., & Wyatt, B. A. (1999). Harzburgite to lherzolite and back again: Metasomatic processes in ultramafic xenoliths from the Wesselton kimberlite, Kimberley, South Africa. *Contributions to Mineralogy and Petrology*, *134*(2-3), 232–250. https://doi.org/10.1007/s004100050481

Grütter, H. S. (2009). Pyroxene xenocryst geotherms: Techniques and application. *Lithos*, *112*, 1167–1178. https://doi.org/10.1016/j.lithos.2009.03.023

Hart, S. R., Blusztajn, J., Dick, H. J. B., Meyer, P. S., & Muehlenbachs, K. (1999). The fingerprint of seawater circulation in a 500-meter section of ocean crust gabbros. *Geochimica Et Cosmochimica Acta*, *63*(23-24), 4059–4080.

Harte, B., & Kirkley, M. B. (1997). Partitioning of trace elements between clinopyroxene and garnet: Data from mantle eclogites. *Chemical Geology*, *136*(1-2), 1–24.

Hasterok, D., & Chapman, D. S. (2011). Heat production and geotherms for the continental lithosphere. *Earth and Planetary Science Letters*, *307*(1-2), 59–70. https://doi.org/10.1016/j.epsl.2011.04.034

Hayman, P. C., Cas, R. A. F., & Johnson, M. (2009). Characteristics and alteration origins of matrix minerals in volcaniclastic kimberlite of the Muskox pipe (Nunavut, Canada). *Lithos*, *112*, 473–487. https://doi.org/10.1016/j.lithos.2009.06.025

Heaman, L. M., Creaser, R. A., & Cookenboo, H. O. (2002). Extreme enrichment of high field strength elements in Jericho eclogite xenoliths: A cryptic record of Paleoproterozoic subduction, partial melting, and metasomatism beneath the Slave craton, Canada. *Geology*, *30*(6), 507–510.

Heaman, L. M., Creaser, R. A., Cookenboo, H. O., & Chacko, T. (2006). Multi-stage modification of the northern Slave mantle lithosphere: Evidence from zircon- and diamond-bearing eclogite xenoliths entrained in Jericho kimberlite, Canada. *Journal of Petrology*, *47*(4), 821–858. https://doi.org/10.1093/petrology.egi097

Heaman, L. M., Kjarsgaard, B. A., & Creaser, R. A. (2004). The temporal evolution of North American kimberlites. *Lithos*, *76*(1-4), 377–397. https://doi.org/10.1016/j.lithos.2004.03.047

Helmstaedt, H., & Schulze, D. J. (1989). Southern African kimberlites and their mantle sample: Implications for Archean tectonics and lithosphere evolution. In R. Rushmer (Ed.), *Evolution and Differentiation of the Continental Crust* (pp. 67–91). Cambridge: Cambridge University Press.

Herzberg, C., & Asimow, P. D. (2008). Petrology of some oceanic island basalts: PRIMELT2.XLS software for primary magma calculation. *Geochemistry Geophysics Geosystems*, *9*. https://doi.org/10.1029/2008gc002057

Hills, D. V., & Haggerty, S. E. (1989). Petrochemistry of eclogites from the Koidu kimberlite complex, Sierra-Leone. *Contributions to Mineralogy and Petrology*, *103*(4), 397–422. https://doi.org/10.1007/bf01041749

Hopp, J., Trieloff, M., Brey, G. P., Woodland, A. B., Simon, N. S. C., Wijbrans, J. R., et al. (2008). 40Ar/39Ar-ages of phlogopite in mantle xenoliths from South African kimberlites: Evidence for metasomatic mantle impregnation during the Kibaran orogenic cycle. *Lithos*, *106*(3-4), 351–364. https://doi.org/10.1016/j.lithos.2008.09.001

Howarth, G. H., Michael, E., Skinner, W., & Prevec, S. A. (2011). Petrology of the hypabyssal kimberlite of the Kroonstad group II kimberlite (orangeite) cluster, South Africa: Evolution of the magma within the cluster. *Lithos*, *125*(1-2), 795–808. https://doi.org/10.1016/j.lithos.2011.05.001

Huang, J. X., Greau, Y., Griffin, W. L., O'Reilly, S. Y., & Pearson, N. J. (2012). Multi-stage origin of Roberts Victor eclogites: Progressive metasomatism and its isotopic effects. *Lithos*, *142-143*, 161–181. https://doi.org/10.1016/j.lithos.2012.03.002

Huang, J. X., Li, P., Griffin, W. L., Xia, Q. K., Greau, Y., Pearson, N. J., & O'Reilly, S. Y. (2014). Water contents of Roberts Victor xenolithic eclogites: Primary and metasomatic controls. *Contributions to Mineralogy and Petrology*, *168*(6), 1092. https://doi.org/10.1007/s00410-014-1092-5

Ireland, T. R., Rudnick, R. L., & Spetsius, Z. (1994). Trace elements in diamond inclusions from eclogites reveal link to Archean granites. *Earth and Planetary Science Letters*, *128*(3-4), 199–213.

Izraeli, E. S., Harris, J. W., & Navon, O. (2001). Brine inclusions in diamonds: A new upper mantle fluid. *Earth and Planetary Science Letters*, *187*(3-4), 323–332. https://doi.org/10.1016/s0012-821x(01)00291-6

Jacob, D. E. (2004). Nature and origin of eclogite xenoliths from kimberlites. *Lithos*, *77*(1-4), 295–316. https://doi.org/10.1016/j.lithos.2004.03.038

Jacob, D. E., Schmickler, B., & Schulze, D. J. (2003). Trace element geochemistry of coesite-bearing eclogites from the Roberts Victor kimberlite, Kaapvaal craton. *Lithos*, *71*(2-4), 337–351. https://doi.org/10.1016/S0024-4937(03)00120-8

Jacob, D. E., Viljoen, K. S., & Grassineau, N. V. (2009). Eclogite xenoliths from Kimberley, South Africa—A case study of mantle metasomatism in eclogites. *Lithos*, *112*, 1002–1013. https://doi.org/10.1016/j.lithos.2009.03.034

Jenner, F. E., & O'Neill, H. S. (2012). Analysis of 60 elements in 616 ocean floor basaltic glasses. *Geochemistry Geophysics Geosystems*, *13*.

Jollands, M. C., Hanger, B. J., Yaxley, G. M., Hermann, J., & Kilburn, M. R. (2018). Timescales between mantle metasomatism and kimberlite ascent indicated by diffusion profiles in garnet crystals from peridotite xenoliths. *Earth and Planetary Science Letters*, *481*, 143–153. https://doi.org/10.1016/j.epsl.2017.10.021

Jones, A. G., Evans, R. L., & Eaton, D. W. (2009). Velocity-conductivity relationships for mantle mineral assemblages in Archean cratonic lithosphere based on a review of laboratory data and Hashin-Shtrikman extremal bounds. *Lithos*, *109*(1-2), 131–143. https://doi.org/10.1016/j.lithos.2008.10.014

Jones, A. G., Ferguson, I. J., Chave, A. D., Evans, R. L., & McNeice, G. W. (2001). Electric lithosphere of the Slave craton. *Geology*, *29*(5), 423–426.

Kelly, R. K., Kelemen, P. B., & Jull, M. (2003). Buoyancy of the continental upper mantle. *Geochemistry Geophysics Geosystems*, *4*(2). https://doi.org/10.1029/2002gc000399

Klemme, S., Vanderlaan, S. R., Foley, S. F., & Gunther, D. (1995). Experimentally-determined trace and minor element partitioning between clinpyroxene and carbonatite melt under upper-mantle conditions. *Earth and Planetary Science Letters*, *133*(3-4), 439–448. https://doi.org/10.1016/0012-821x(95)00098-w

Knapp, N., Woodland, A. B., & Klimm, K. (2015). Experimental constraints on coesite abundances in eclogite and implications for the X seismic discontinuity. *Journal of Geophysical Research-Solid Earth*, *120*(7), 4917–4930. https://doi.org/10.1002/2015jb011933

Kobussen, A. F., Griffin, W. L., & O'Reilly, S. Y. (2009). Cretaceous thermo-chemical modification of the Kaapvaal cratonic lithosphere, South Africa. *Lithos*, *112*, 886–895. https://doi.org/10.1016/j.lithos.2009.06.031

Kolesnichenko, M. V., Zedgenizov, D. A., Ragozin, A. L., Litasov, K. D., & Shatsky, V. S. (2018). The role of eclogites in the redistribution of water in the subcontinental mantle of the Siberian craton: Results of determination of the water content in minerals from the Udachnaya pipe eclogites. *Russian Geology and Geophysics*, *59*(7), 763–779. https://doi.org/10.1016/j.rgg.2018.07.004

Kopylova, M. G., Beausoleil, Y., Goncharov, A., Burgess, J., & Strand, P. (2016). Spatial distribution of eclogite in the Slave cratonic mantle: The role of subduction. *Tectonophysics*, *672-673*, 87–103. https://doi.org/10.1016/j.tecto.2016.01.034

Kopylova, M. G., Lo, J., & Christensen, N. I. (2004). Petrological constraints on seismic properties of the Slave upper mantle (Northern Canada). *Lithos*, *77*(1-4), 493–510. https://doi.org/10.1016/j.lithos.2004.03.012

Korolev, N. M., Melnik, A. E., Li, X. H., & Skublov, S. G. (2018). The oxygen isotope composition of mantle eclogites as a proxy of their origin and evolution: A review. *Earth-Science Reviews*, *185*, 288–300. https://doi.org/10.1016/j.earscirev.2018.06.007

Krogh, E. J. (1988). The garnet-clinopyroxene Fe-Mg geothermometer—A reinterpretation of existing experimental data. *Contributions to Mineralogy and Petrology*, *99*(1), 44–48. https://doi.org/10.1007/BF00399364

Krogh Ravna, E. J. (2000). The garnet-clinopyroxene $Fe2^{+}$-Mg geothermometer: An updated calibration. *Journal of Metamorphic Geology*, *18*(2), 211–219. https://doi.org/10.1046/j.1525-1314.2000.00247.x

Le Roex, A. P., Bell, D. R., & Davis, P. (2003). Petrogenesis of group I kimberlites from Kimberley, South Africa: Evidence from bulk-rock geochemistry. *Journal of Petrology*, *44*(12), 2261–2286. https://doi.org/10.1093/petrology/egg077

Lee, C. T. A., Cheng, X., & Horodyskyj, U. (2006). The development and refinement of continental arcs by primary basaltic magmatism, garnet pyroxenite accumulation, basaltic recharge and delamination: Insights from the Sierra Nevada, California. *Contributions to Mineralogy and Petrology*, *151*(2), 222–242. https://doi.org/10.1007/s00410-005-0056-1

Lee, C. T. A., Luffi, P., & Chin, E. J. (2011). Building and destroying continental mantle. In R. Jeanloz & K. H. Freeman (Eds.), *Annual Review of Earth and Planetary Sciences, Vol 39* (Vol. 39, pp. 59–90). Palo Alto, CA: Annual Reviews.

Liu, H., Zhu, Q., & Yang, X. (2019). Electrical conductivity of OH-bearing omphacite and garnet in eclogite: The quantitative dependence on water content. *Contrib Mineral Petrol*, *174*(7), 57. https://doi.org/10.1007/s00410-019-1593-3

Luth, R. W., & Stachel, T. (2014). The buffering capacity of lithospheric mantle: Implications for diamond formation. *Contributions to Mineralogy and Petrology*, *168*(5), 1083. https://doi.org/10.1007/s00410-014-1083-6

MacGregor, I. D., & Carter, J. L. (1970). The chemistry of clinopyroxenes and garnets of eclogite and peridotite xenoliths from the Roberts Victor mine, South Africa. *Physics of the Earth and Planetary Interiors*, *3*, 391–397. https://doi.org/10.1016/0031-9201(70)90081-6

Mallik, A., & Dasgupta, R. (2013). Reactive infiltration of MORB-eclogite-derived carbonated silicate melt into fertile peridotite at 3 GPa and genesis of alkalic magmas. *Journal of Petrology*, *54*(11), 2267–2300. https://doi.org/10.1093/petrology/egt047

Marshall, E. W., Lassiter, J. C., & Barnes, J. D. (2018). On the (mis)behavior of water in the mantle: Controls on nominally anhydrous mineral water content in mantle peridotites. *Earth and Planetary Science Letters*, *499*, 219–229. https://doi.org/10.1016/j.epsl.2018.07.033

Mather, K. A. (2012). *A xenolith-based lithospheric transect of the Slave craton, N.W.T., Canada*. Durham: (Doctor of Philosophy), Durham University.

Mattey, D., Lowry, D., & Macpherson, C. (1994). Oxygen-isotope composition of mantle peridotite. *Earth and Planetary Science Letters*, *128*(3-4), 231–241. https://doi.org/10.1016/0012-821x(94)90147-3

McCandless, T. E., & Gurney, J. J. (1989). Sodium in garnet and potassium in clinopyroxene: Criteria for classifying mantle eclogites. In J. Ross, A. L. Jacques, J. Ferguson, D. H. Green, S. Y. O'Reilly, R. V. Danchin, & A. J. A. Janse (Eds.), *Kimberlites and Related Rocks, Vol 2. Their Mantle/Crust Setting, Diamonds and Diamond Exploration* (Vol. 14, pp. 827–832). Hornsby: Carlton: Geological Society of Australia Special Publication No. 14. Blackwell Scientific.

McLean, H., Banas, A., Creighton, S., Whiteford, S., Luth, R. W., & Stachel, T. (2007). Garnet xenocrysts from the Diavik mine, NWT, Canada: Composition, color, and paragenesis. *Canadian Mineralogist*, *45*, 1131–1145.

Miensopust, M. P., Jones, A. G., Muller, M. R., Garcia, X., & Evans, R. L. (2011). Lithospheric structures and Precambrian terrane boundaries in northeastern Botswana revealed through magnetotelluric profiling as part of the Southern African Magnetotelluric Experiment. *Journal of Geophysical Research-Solid Earth*, 116. https://doi.org/10.1029/2010jb007740

Misra, K. C., Anand, M., Taylor, L. A., & Sobolev, N. V. (2004). Multi-stage metasomatism of diamondiferous eclogite xenoliths from the Udachnaya kimberlite pipe, Yakutia, Siberia. *Contributions to Mineralogy and Petrology*, *146*(6), 696–714. https://doi.org/10.1007/s00410-003-0529-z

Mitchell, R. H. (2006). Potassic magmas derived from metasomatized lithospheric mantle: Nomenclature and relevance to exploration for diamond-bearing rocks. *Journal of the Geological Society of India*, *67*(3), 317–327.

Morimoto, N., Gabries, J., Ferguson, A. K., Ginzburg, I. V., Ross, M., Seifert, F. A., et al. (1988). Nomenclature of pyroxenes. *American Mineralogist*, *73*, 1123–1133.

Moss, S. W., Kobussen, A., Powell, W., & Pollock, K. (2018). Kimberlite emplacement and mantle sampling through time at A154N kimberlite volcano, Diavik Diamond Mine: Lessons from the deep. *Mineralogy and Petrology*, *112*, 397–410. https://doi.org/10.1007/s00710-018-0630-7

Muehlenbachs, K., & Clayton, R. N. (1972a). Oxygen isotope studies of fresh and weathered submarine basalts. *Canadian Journal of Earth Sciences*, *9*(2), 172–184.

Muehlenbachs, K., & Clayton, R. N. (1972b). Oxygen isotope geochemistry of submarine greenstones. *Canadian Journal of Earth Sciences*, *9*(5), 471–478.

Nikitina, L. P., Korolev, N. M., Zinchenko, V. N., & Felix, J. T. (2014). Eclogites from the upper mantle beneath the Kasai Craton (Western Africa): Petrography, whole-rock geochemistry and U-Pb zircon age. *Precambrian Research*, *249*, 13–32.

O'Reilly, S. Y., & Griffin, W. L. (1995). Trace-element partitioning between garnet and clinopyroxene in mantle-derived pyroxenites and eclogites: P-T-X controls. *Chemical Geology*, *121*, 105–130.

O'Reilly, S. Y., & Griffin, W. L. (2013). Mantle metasomatism. In D. E. Harlov, & H. Austrheim (Eds.), *Metasomatism and the Chemical Transformation of Rock* (pp. 471–533). Berlin Heidelberg: Springer Verlag.

Pan, S., Zheng, J., Yin, Z., Griffin, W. L., Xia, M., Lin, A., & Zhang, H. (2018). Spongy texture in mantle clinopyroxene records decompression-induced melting. *Lithos*, *320-321*, 144–154.

Patten, C., Barnes, S. J., Mathez, E. A., & Jenner, F. E. (2013). Partition coefficients of chalcophile elements between sulfide and silicate melts and the early crystallization history of sulfide liquid: LA-ICP-MS analysis of MORB sulfide droplets. *Chemical Geology*, *358*, 170–188. https://doi.org/10.1016/j.chemgeo.2013.08.040

Poli, S. (2015). Carbon mobilized at shallow depths in subduction zones by carbonatitic liquids. *Nature Geoscience*, *8*(8), 633. https://doi.org/10.1038/ngeo2464

Pollack, H. N., & Chapman, D. S. (1977). On the regional variation of heat-flow, geotherms, and lithospheric thickness. *Tectonophysics*, *38*(3-4), 279–296.

Pyle, J. M., & Haggerty, S. E. (1998). Eclogites and the metasomatism of eclogites from the Jagersfontein Kimberlite: Punctuated transport and implications for alkali magmatism. *Geochimica Et Cosmochimica Acta*, *62*(7), 1207–1231. https://doi.org/10.1016/s0016-7037(98)00040-4

Rader, E., Emry, E., Schmerr, N., Frost, D., Cheng, C., Menard, J., et al. (2015). Characterization and petrological constraints of the mid-lithospheric discontinuity. *Geochemistry Geophysics Geosystems*, *16*(10), 3484–3504. https://doi.org/10.1002/2015gc005943

Radu, I. B., Harris, C., Moine, B. N., Costin, G., & Cottin, J. Y. (2019). Subduction relics in the subcontinental lithospheric mantle evidence from variation in the O-18 value of eclogite xenoliths from the Kaapvaal craton. *Contributions to Mineralogy and Petrology*, *174*(3). https://doi.org/10.1007/s00410-019-1552-z

Riches, A. J. V., Ickert, R. B., Pearson, D. G., Stern, R. A., Jackson, S. E., Ishikawa, A., et al. (2016). In situ oxygen-isotope, major-, and trace-element constraints on the metasomatic modification and crustal origin of a diamondiferous eclogite from Roberts Victor, Kaapvaal Craton. *Geochimica Et Cosmochimica Acta*, *174*, 345–359. https://doi.org/10.1016/j.gca.2015.11.028

Roden, M. F., & Murthy, R. V. (1985). Mantle metasomatism. *Annual Review of Earth and Planetary Sciences*, *13*(1), 269–296. https://doi.org/10.1146/annurev.ea.13.050185.001413

Rudnick, R. L., & Fountain, D. M. (1995). Nature and composition of the continental crust: A lower crustal perspective. *Reviews of Geophysics*, *33*(3), 267–309. https://doi.org/10.1029/95rg01302

Rudnick, R. L., & Nyblade, A. (1999). The thickness and heat production of Archean lithosphere: Constraints from xenolith thermobarometry and surface heat flow. In Y. Fei, C. Bertka, & B. Mysen (Eds.), *Mantle Petrology: Field Observations and High Pressure Experimentation: A Tribute to Francis R. (Joe) Boyd*. Special Publication No. 6 (pp. 3–12). Houston TX: Geochemical Society.

Russell, J. K., Dipple, G. M., & Kopylova, M. G. (2001). Heat production and heat flow in the mantle lithosphere, Slave craton, Canada. *Physics of the Earth and Planetary Interiors*, *123*(1), 27–44. https://doi.org/10.1016/s0031-9201(00)00201-6

Schmidberger, S. S., Simonetti, A., Heaman, L. M., Creaser, R. A., & Whiteford, S. (2007). Lu-Hf, in-situ Sr and Pb isotope and trace element systematics for mantle eclogites from the Diavik diamond mine: Evidencefor Paleoproterozoic subduction beneath the Slave craton, Canada. *Earth and Planetary Science Letters*, *254*(1-2), 55–68. https://doi.org/10.1016/j.epsl.2006.11.020

Schulze, D. J., Wiese, D., & Steude, J. (1996). Abundance and distribution of diamonds in eclogite revealed by volume visualization of CT X-ray scans. *Journal of Geology*, *104*(1), 109–114.

Selway, K. (2014). On the causes of electrical conductivity anomalies in tectonically stable lithosphere. *Surveys in Geophysics*, *35*(1), 219–257. https://doi.org/10.1007/s10712-013-9235-1

Shatsky, V., Ragozin, A., Zedgenizov, D., & Mityukhin, S. (2008). Evidence for multistage evolution in a xenolith of diamond-bearing eclogite from the Udachnaya kimberlite pipe. *Lithos*, *105*(3-4), 289–300. https://doi.org/10.1016/j.lithos.2008.04.008

Shchukina, E. V., Agashev, A. M., & Zedgenizov, D. A. (2018). Origin of zircon-bearing mantle eclogites entrained in the V. Grib kimberlite (Arkhangelsk region, NW Russia): Evidence from mineral geochemistry and the U-Pb and Lu-Hf isotope compositions of zircon. *Mineralogy and Petrology*, *112*, 85–100. https://doi.org/10.1007/s00710-018-0581-z

Shirey, S. B., & Richardson, S. H. (2011). Start of the Wilson cycle at 3 Ga shown by diamonds from subcontinental mantle. *Science*, *333*(6041), 434–436. https://doi.org/10.1126/science.1206275

Shu, Q., Brey, G. P., & Pearson, D. G. (2018). Eclogites and garnet pyroxenites from Kimberley, Kaapvaal craton, South Africa: Their diverse origins and complex metasomatic signatures. *Mineralogy and Petrology*, *112*, 43–56. https://doi.org/10.1007/s00710-018-0595-6

Skinner, E. M. W., Apter, D. B., Morelli, C., & Smithson, N. K. (2004). Kimberlites of the Man craton, West Africa. *Lithos*, *76*(1-4), 233–259. https://doi.org/10.1016/j.lithos.2004.04.034

Smart, K. A., Chacko, T., Simonetti, A., Sharp, Z. D., & Heaman, L. M. (2014). A record of paleoproterozoic subduction preserved in the northern Slave cratonic mantle: Sr-Pb-O isotope and trace-element investigations of eclogite xenoliths from the Jericho and Muskox kimberlites. *Journal of Petrology*, *55*(3), 549–583. https://doi.org/10.1093/petrology/egt077

Smart, K. A., Chacko, T., Stachel, T., Tappe, S., Stern, R. A., Ickert, R. B., & Eimf (2012). Eclogite formation beneath the northern Slave craton constrained by diamond inclusions: Oceanic lithosphere origin without a crustal signature. *Earth and Planetary Science Letters*, *319*, 165–177. https://doi.org/10.1016/j.epsl.2011.12.032

Smart, K. A., Heaman, L. M., Chacko, T., Simonetti, A., Kopylova, M., Mah, D., & Daniels, D. (2009). The origin of high-MgO diamond eclogites from the Jericho Kimberlite, Canada. *Earth and Planetary Science Letters*, *284*(3-4), 527–537. https://doi.org/10.1016/j.epsl.2009.05.020

Smart, K. A., Tappe, S., Simonetti, A., Simonetti, S. S., Woodland, A. B., & Harris, C. (2017). Tectonic significance and redox state of Paleoproterozoic eclogite and pyroxenite components in the Slave cratonic mantle lithosphere, Voyageur kimberlite, Arctic Canada. *Chemical Geology*, *455*, 98–119. https://doi.org/10.1016/j.chemgeo.2016.10.014

Smit, K. V., Shirey, S. B., & Wang, W. Y. (2016). Type Ib diamond formation and preservation in the West African lithospheric mantle: Re-Os age constraints from sulphide inclusions in Zimmi diamonds. *Precambrian Research*, *286*, 152–166. https://doi.org/10.1016/j.precamres.2016.09.022

Smit, K. V., Stachel, T., Creaser, R. A., Ickert, R. B., DuFrane, S. A., Stern, R. A., & Seller, M. (2014). Origin of eclogite and pyroxenite xenoliths from the Victor kimberlite, Canada, and implications for Superior craton formation. *Geochimica Et Cosmochimica Acta*, *125*, 308–337. https://doi.org/10.1016/j.gca.2013.10.019

Smit, K. V., Stachel, T., Luth, R. W., & Stern, R. A. (2019). Evaluating mechanisms for eclogitic diamond growth: An example from Zimmi Neoproterozoic diamonds (West African craton). *Chemical Geology*, *520*, 21–32.

Sokol, A. G., Kupriyanov, I. N., Palyanov, Y. N., Kruk, A. N., & Sobolev, N. V. (2013). Melting experiments on the Udachnaya kimberlite at 6.3–7.5 GPa: Implications for the role of H2O in magma generation and formation of hydrous olivine. *Geochimica Et Cosmochimica Acta*, *101*, 133–155. https://doi.org/10.1016/j.gca.2012.10.018

Spetsius, Z. V., & Taylor, L. A. (2002). Partial melting in mantle eclogite xenoliths: Connections with diamond paragenesis. *International Geology Review*, *44*(11), 973–987. https://doi.org/10.2747/0020-6814.44.11.973

Stachel, T., & Luth, R. W. (2015). Diamond formation—Where, when and how? *Lithos*, *220*, 200–220. https://doi.org/10.1016/j.lithos.2015.01.028

Stagno, V., Frost, D. J., McCammon, C. A., Mohseni, H., & Fei, Y. (2015). The oxygen fugacity at which graphite or diamond forms from carbonate-bearing melts in eclogitic rocks. *Contributions to Mineralogy and Petrology*, *169*(2), 16. https://doi.org/10.1007/s00410-015-1111-1

Stagno, V., Ojwang, D. O., McCammon, C. A., & Frost, D. J. (2013). The oxidation state of the mantle and the extraction of carbon from Earth's interior. *Nature*, *493*(7430), 84–88.

Stamm, N., & Schmidt, M. W. (2017). Asthenospheric kimberlites: Volatile contents and bulk compositions at 7 GPa. *Earth and Planetary Science Letters*, *474*, 309–321.

Staudigel, H. (2005). Hydrothermal alteration processes in the oceanic crust. In H. D. Holland, & K. K. Turekian (Eds.), *Treatise on Geochemistry. The Crust* (pp. 511–535). Amsterdam: Elsevier/Pergamon.

Stiefenhofer, J., Viljoen, K. S., & Marsh, J. S. (1997). Petrology and geochemistry of peridotite xenoliths from the Letlhakane kimberlites, Botswana. *Contributions to Mineralogy and Petrology*, *127*(1-2), 147–158.

Stixrude, L., & Lithgow-Bertelloni, C. (2005). Thermodynamics of mantle minerals—I. *Physical properties, Geophysical Journal International*, *162*, 610–631.

Stixrude, L., & Lithgow-Bertelloni, C. (2011). Thermodynamics of mantle minerals—II. *Phase equilibria, Geophysical Journal International*, *184*, 1180–1213.

Sun, S.-S., & McDonough, W. F. (1989). Chemical and isotopc systematics of oceanic basalts: Implications for mantle composition and processes. In A. D. Saunders, M. J. Norry, & D. S. A. M. J. Norr (Eds.), *Magmatism in the Ocean Basins* (pp. 313–345). London: Geological Society.

Szumila, I., Trail, D., & Danielson, L. (2019). The effect of fO(2) on the diffusion of redox-sensitive elements in haplobasaltic melt at 1 GPa and 1300 °C. *Chemical Geology*, *512*, 107–120. https://doi.org/10.1016/j.chemgeo.2019.02.018

Tappe, S., Brand, N. B., Stracke, A., van Acken, D., Liu, C. Z., Strauss, H., et al. (2017). Plates or plumes in the origin of kimberlites: U/Pb perovskite and Sr-Nd-Hf-Os-C-O isotope constraints from the Superior craton (Canada). *Chemical Geology*, *455*, 57–83. https://doi.org/10.1016/j.chemgeo.2016.08.019

Tappe, S., Foley, S. F., Kjarsgaard, B. A., Romer, R. L., Heaman, L. M., Stracke, A., & Jenner, G. A. (2008). Between carbonatite and lamproite—Diamondiferous Torngat ultramafic lamprophyres formed by carbonate-fluxed melting of cratonic MARID-type metasomes. *Geochimica Et Cosmochimica Acta*, *72*(13), 3258–3286. https://doi.org/10.1016/j.gca.2008.03.008

Tappe, S., Pearson, D. G., Kjarsgaard, B. A., Nowell, G., & Dowall, D. (2013). Mantle transition zone input to kimberlite magmatism near a subduction zone: Origin of anomalous Nd-Hf isotope systematics at Lac de Gras, Canada. *Earth and Planetary Science Letters*, *371*, 235–251. https://doi.org/10.1016/j.epsl.2013.03.039

Taylor, L. A., Keller, R. A., Snyder, G. A., Wang, W. Y., Carlson, W. D., Hauri, E. H., et al. (2000). Diamonds and their mineral inclusions, and what they tell us: A detailed "pull-apart" of a diamondiferous eclogite. *International Geology Review*, *42*(11), 959–983.

Taylor, L. A., Milledge, H. J., Bulanova, G. P., Snyder, G. A., & Keller, R. A. (1998). Metasomatic eclogitic diamond growth: Evidence from multiple diamond inclusions. *International Geology Review*, *40*(8), 663–676.

Taylor, L. A., Snyder, G. A., Crozaz, G., Sobolev, V. N., Yefimova, E. S., & Sobolev, N. V. (1996). Eclogitic inclusions in diamonds: Evidence of complex mantle processes over time. *Earth and Planetary Science Letters*, *142*(3-4), 535–551.

Timmerman, S., Koornneef, J. M., Chinn, I. L., & Davies, G. R. (2017). Dated eclogitic diamond growth zones reveal variable recycling of crustal carbon through time. *Earth and Planetary Science Letters*, *463*, 178–188. https://doi.org/10.1016/j.epsl.2017.02.001

Tumiati, S., Tiraboschi, C., Sverjensky, D. A., Pettke, T., Recchia, S., Ulmer, P., et al. (2017). Silicate dissolution boosts the CO_2 concentrations in subduction fluids. *Nature Communications*, *8*(1), 616. https://doi.org/10.1038/s41467-017-00562-z

Viljoen, K. S., Schulze, D. J., & Quadling, A. G. (2005). Contrasting group I and group II eclogite xenolith petrogenesis: Petrological, trace element and isotopic evidence from eclogite, garnet-websterite and alkremite xenoliths in the Kaalvallei kimberlite, South Africa. *Journal of Petrology*, *46*(10), 2059–2090. https://doi.org/10.1093/petrology/egi047

Viljoen, K. S., Smith, C. B., & Sharp, Z. D. (1996). Stable and radiogenic isotope study of eclogite xenoliths from the Orapa kimberlite, Botswana. *Chemical Geology*, *131*(1-4), 235–255.

Weiss, Y., Kessel, R., Griffin, W. L., Kiflawi, I., Klein-BenDavid, O., Bell, D. R., et al. (2009). A new model for the evolution of diamond-forming fluids: Evidence from microinclusion-bearing diamonds from Kankan, Guinea. *Lithos*, *112*, 660–674. https://doi.org/10.1016/j.lithos.2009.05.038

Weiss, Y., McNeill, J., Pearson, D. G., Nowell, G. M., & Ottley, C. J. (2015). Highly saline fluids from a subducting slab as the source for fluid-rich diamonds. *Nature*, *524*(7565), 339–342. https://doi.org/10.1038/nature14857

Xu, J. G., Zhang, D. Z., Fan, D. W., Dera, P. K., Shi, F., & Zhou, W. G. (2019). Thermoelastic properties of eclogitic garnets and omphacites: Implications for deep subduction of oceanic crust and density anomalies in the upper mantle. *Geophysical Research Letters*, *46*(1), 179–188. https://doi.org/10.1029/2018gl081170

Yang, X. Z., Keppler, H., McCammon, C., Ni, H. W., Xia, Q. K., & Fan, Q. C. (2011). Effect of water on the electrical conductivity of lower crustal clinopyroxene. *Journal of Geophysical Research-Solid Earth*, *116*(B4), B04208. https://doi.org/10.1029/2010JB008010

Yaxley, G. M., Berry, A. J., Rosenthal, A., Woodland, A. B., & Paterson, D. (2017). Redox preconditioning deep cratonic lithosphere for kimberlite genesis—Evidence from the central Slave Craton. *Scientific Reports*, *7*. https://doi.org/10.1038/s41598-017-00049-3

Zedgenizov, D. A., Ragozin, A. L., Shatsky, V. S., & Griffin, W. L. (2018). Diamond formation during metasomatism of mantle eclogite by chloride-carbonate melt. *Contributions to Mineralogy and Petrology*, *173*(10). https://doi.org/10.1007/s00410-018-1513-y

Zhao, C. C., & Yoshino, T. (2016). Electrical conductivity of mantle clinopyroxene as a function of water content and its implication on electrical structure of uppermost mantle. *Earth and Planetary Science Letters*, *447*, 1–9. https://doi.org/10.1016/j.epsl.2016.04.028